

Centrality dependence of kinetic freeze-out temperature and transverse flow velocity in high energy nuclear collisions

Muhammad Waqas^{1,2,3,*}, Fu-Hu Liu^{1,2,†}

¹*Institute of Theoretical Physics & State Key Laboratory of Quantum Optics and Quantum Optics Devices, Shanxi University, Taiyuan 030006, Shanxi, People's Republic of China*

²*Collaborative Innovation Center of Extreme Optics, Shanxi University, Taiyuan 030006, Shanxi, People's Republic of China*

³*School of Nuclear Science and Technology, University of Chinese Academy of Sciences, Beijing 100049, People's Republic of China*

Abstract: Centrality-dependent double-differential transverse momentum spectra of charged pions, kaons, and (anti)protons produced in mid-pseudorapidity interval in $\sqrt{s_{NN}} = 200$ GeV gold-gold and deuteron-gold collisions with different centralities are analyzed by the blast-wave model with Boltzmann-Gibbs statistics. Meanwhile, the mentioned spectra in mid-rapidity interval in $\sqrt{s_{NN}} = 2.76$ TeV lead-lead and $\sqrt{s_{NN}} = 5.02$ TeV proton-lead collisions with different centralities are analyzed by the same model. The model results are approximately in agreement with the experimental data in special transverse momentum ranges. It is shown that with the increase of event centrality and energy, the kinetic freeze-out temperature of the emission source and the transverse flow velocity of the produced particles slightly increase in some cases but they do not give an obvious change in other cases. Meanwhile, the kinetic freeze-out temperature (transverse flow velocity) increases (decreases) with the increase of particle mass. The average transverse momentum and initial temperature increase with the increase of event centrality, collision energy, and particle mass. This work also confirms the maximum size dependent effect, which states that the main parameters such as the kinetic freeze-out temperature and transverse flow velocity are mainly determined by the heaviest nucleus from proton-nucleus to nucleus-nucleus collisions.

Keywords: Centrality dependence, kinetic freeze-out temperature, transverse flow velocity

PACS: 12.40.Ee, 14.40.Aq, 24.10.Pa, 25.75.Ag

1 Introduction

The kinetic freeze-out temperature (T_0 or T_{kin}) of emission source and the transverse flow velocity (β_T) of produced particles are two important quantities at the stage of kinetic freeze-out which is the last stage in high energy proton-proton, proton-nucleus, and nucleus-nucleus collisions [1, 2, 3], where T_0 and β_T reflect the thermal motion of produced particles and the collective expansion of emission source respectively. From the initial stage to the last stage, the interacting system undergoes different stages among which there is the stage of chemical freeze-out. It is expected that the freeze-out parameters are event centrality and collision energy dependent due to the fact that the violent degree of impact is related to the amount of energy deposition which results in given excitation and expansion degrees of the system. In particular, the event centrality dependent freeze-out parameters at given collision energy can be studied in proton-nucleus and nucleus-nucleus collisions. Although, the proton-proton collisions are not

considered in the present work, the centrality of proton-proton collisions can be also determined by particle multiplicity.

As the result of soft excitation process, the transverse momentum (p_T) spectra of charged particles in low p_T region contain information of T_0 and β_T [1, 2, 3]. There are multiple methods to extract T_0 and β_T . These methods include the blast-wave model with Boltzmann-Gibbs [1, 2, 3] or Tsallis statistics [4], the alternative method using the Boltzmann [2, 5, 6, 7, 8, 9, 10, 11] or Tsallis distribution [12, 13], etc. The Boltzmann-Gibbs statistics and Boltzmann distribution are our preferred methods due to their similarity with the ideal gas model in thermodynamics.

We can select the methods that used the Boltzmann-Gibbs statistics and Boltzmann distribution [1, 2, 3] to describe the spectra in low p_T region which is less than 2–3 GeV/c in peripheral collisions and 4.5 GeV/c or a little more in central collisions. However, these methods are not suitable for the spectra in high p_T region

*E-mail: waqas_phy313@yahoo.com

†Corresponding author. E-mail: fuhuliu@163.com; fuhuliu@sxu.edu.cn

which needs the description of other methods such as the Hagedorn function [14, 15] due to the contribution of hard scattering process. As a probability density function, the Hagedorn function can contribute in both the low and high p_T regions. That is, except for the disengaging of T_0 and β_T in the extraction process, we should exclude the contribution of the hard process in low p_T region. Comparatively higher values for T_0 and β_T will be obtained, if the hard process available in the Hagedorn model [14] is included in low p_T region where it's relative fraction is small and the departure caused by the hard process can be neglected as well. In other words, we would like to say that we can neglect contribution of hard process in low p_T region, when extracting T_0 and β_T parameters.

In the present work, the centrality-dependent double-differential transverse momentum spectra of charged pions produced in high energy nuclear collisions will be analyzed by the blast-wave model with Boltzmann-Gibbs statistics [1, 2, 3]. The model results are compared with the experimental data measured by the PHENIX Collaboration in mid-pseudorapidity interval in gold-gold (Au-Au) [16] and deuteron-gold (d -Au) [17] collisions at $\sqrt{s_{NN}} = 200$ GeV with different centralities at the Relativistic Heavy Ion Collider (RHIC), and lead-lead (Pb-Pb) collisions at $\sqrt{s_{NN}} = 2.76$ TeV [18] and proton-lead (p -Pb) collisions at $\sqrt{s_{NN}} = 5.02$ TeV [19] by the ALICE Collaboration in mid-rapidity interval with different centralities at the Large Hadron Collider (LHC).

The remainder of this paper is structured as follows. The method is shortly described in Section 2. Results and discussion are given in Section 3. In Section 4, we summarize our main observations and conclusions

2 The method

The p_T spectra of charged particles produced in high energy collisions have complex structures. To describe the p_T spectra, it is not enough to use only one probability density function, though this function can be of various forms. In particular, the maximum p_T reaches 100 GeV/ c in collisions at the LHC [20]. The model analysis has observed several p_T regions [21] which include the first region with $p_T < 4$ –6 GeV/ c , the second region with 4 –6 GeV/ $c < p_T < 17$ –20 GeV/ c , and the third region with $p_T > 17$ –20 GeV/ c . At the RHIC, the boundaries of different p_T regions are slightly lower. It is expected that different p_T regions correspond to different interacting mechanisms. Even for the same p_T region, different explanations are existed due to different model methods and microcosmic pictures.

According to ref. [21], different p_T regions reflect different whole features of fragmentation and hadroniza-

tion of partons through the string dynamics. In the first p_T region, the effects and changes by the medium take part in the main role. However, it appears weakly in the second p_T region. Meanwhile, the nuclear transparency results in negligible influence of the medium in the third p_T region. From the number of strings point of view, the second p_T region is expected to have the maximum number of strings, which results in fusion and creation of strings and collective behavior of partons. Through string fusion, the second p_T region is proposed as a possible area of Quark-Gluon Plasma (QGP). While, the first p_T region has the minimum number of strings and maximum number of hadrons due to direct hadronization of the low energy strings into mesons [21].

We have used the idea of multiple p_T regions and our explanation in the following paragraphs is somehow different from that in ref. [21]. We regard the first p_T region as the contribution region of soft excitation process. The second and third p_T regions are regarded as the contribution regions of hard and very-hard (VH) scattering processes respectively. Considering the contribution region ($p_T < 0.2$ –0.3 GeV/ c) of very-soft (VS) excitation process due to resonant production of charged pions in some cases, we have one more p_T region. The four p_T regions can be described by different components in a unified superposition. To structure the unified superposition, we have two methods. The first method is the common method of overlapping of the contribution regions of different components, while the second method is the Hagedorn model [14] which doesn't include this overlapping.

Let $f_S(p_T)$, $f_H(p_T)$, $f_{VS}(p_T)$, and $f_{VH}(p_T)$ denote the probability density functions contributed by the soft, hard, very-soft, and very-hard components, respectively, where $f_{VS}(p_T)$ and $f_{VH}(p_T)$ are assumed to have the same forms as $f_S(p_T)$ and $f_H(p_T)$ with smaller and larger parameters respectively. Then, according to the first method, we can structure the unified superposition to be

$$f_0(p_T) = k_{VS}f_{VS}(p_T) + kf_S(p_T) + (1 - k - k_{VS} - k_{VH})f_H(p_T) + k_{VH}f_{VH}(p_T), \quad (1)$$

where k_{VS} , k_{VH} , and k denote the contribution fractions of the very-soft, very-hard, and soft components respectively.

According to the Hagedorn's model [14], we can use the usual step function to structure the unified superposition. That is

$$f_0(p_T) = A_{VS}\theta(p_{VS} - p_T)f_{VS}(p_T) + A_S\theta(p_T - p_{VS})\theta(p_1 - p_T)f_S(p_T) + A_H\theta(p_T - p_1)\theta(p_{VH} - p_T)f_H(p_T) + A_{VH}\theta(p_T - p_{VH})f_{VH}(p_T), \quad (2)$$

where A_{VS} , A_S , A_H , and A_{VH} are constants which result in the two contiguous components to be equal to each other at $p_T = p_{VS}$, p_1 , and p_{VH} respectively. In particular, p_1 and p_{VH} correspond to 4–6 GeV/c and 17–20 GeV/c in ref. [14] respectively, though the real values may be different from them. Meanwhile, the real values are possibly event centrality and collision energy dependent.

In most cases, the contributions of very-soft and very-hard components can be neglected. Or, the two contributions can be included in soft and hard components respectively. Thus, Eqs. (1) and (2) are simplified to

$$f_0(p_T) = k f_S(p_T) + (1 - k) f_H(p_T) \quad (3)$$

and

$$f_0(p_T) = A_S \theta(p_1 - p_T) f_S(p_T) + A_H \theta(p_T - p_1) f_H(p_T) \quad (4)$$

respectively. The two simplified functions are the same to our recent work [22] which studies the possible scenarios for single, double, or multiple kinetic freeze-out in high energy collisions, though p_T spectra of different types of particles produced in central and peripheral nuclear collisions and proton-proton collisions are analyzed. Various potential functions can be chosen for $f_S(p_T)$ and $f_H(p_T)$, which includes, but are not limited to, the blast-wave model with Boltzmann-Gibbs statistics [1, 2, 3] and the Hagedorn function [14, 15].

According to refs. [1, 2, 3], the blast-wave model with Boltzmann-Gibbs statistics results in the p_T distribution to be

$$f_S(p_T) = C_0 p_T m_T \int_0^R r dr \times I_0 \left[\frac{p_T \sinh(\rho)}{T_0} \right] K_1 \left[\frac{m_T \cosh(\rho)}{T_0} \right], \quad (5)$$

where C_0 is the normalized constant, $m_T = \sqrt{p_T^2 + m_0^2}$ is the transverse mass, m_0 is the rest mass of the considered particle, r and R are the radial position and the maximum radial position in the thermal source, I_0 and K_1 are the modified Bessel functions of the first and second kinds respectively. In the modified Bessel functions, $\rho = \tanh^{-1}[\beta(r)]$ is the boost angle, $\beta(r) = \beta_S (r/R)^{n_0}$ is a self-similar flow profile, β_S is the flow velocity on the surface, $n_0 = 2$ as used in ref. [1]. In particular, $\beta_T = (2/R^2) \int_0^R r \beta(r) dr = 2\beta_S / (n_0 + 2) = 0.5\beta_S$.

The Hagedorn function [14, 15] is known as an inverse power-law [23, 24, 25],

$$f_H(p_T) = A p_T \left(1 + \frac{p_T}{p_0} \right)^{-n}, \quad (6)$$

where p_0 and n are free parameters and A is the normalization constant. In literature [26], [27, 28, 29, 30, 31],

and [32], the Hagedorn function are revised to

$$f_H(p_T) = A \frac{p_T^2}{m_T} \left(1 + \frac{p_T}{p_0} \right)^{-n}, \quad (7)$$

$$f_H(p_T) = A p_T \left(1 + \frac{p_T^2}{p_0^2} \right)^{-n}, \quad (8)$$

and

$$f_H(p_T) = A \left(1 + \frac{p_T^2}{p_0^2} \right)^{-n}, \quad (9)$$

respectively, where all the three A , p_0 , and n are severally different from each other.

The first method can be changed into the second method (which results in the Hagedorn model [14], if the contribution of hard component in the former method can be neglected in low p_T region due to its small value. If we analyze the spectra in low p_T region, the second component in Eqs. (3) and (4) should be given up due to less contribution of T_0 and β_T in hard component. That is, we can use directly $f_S(p_T)$ from Eq. (5) which also includes the contribution of very-soft component that comes from resonance decays if available in the data. In this work, the contribution of hard component in low p_T region if available is not excluded in the extraction of T_0 and β_T . This treatment causes a slight increase in T_0 and/or β_T in which the relative increase is neglected due to small value ($< 5\%$) [33].

Although we use only Eq. (5) but Eqs. (3) and (4) are kept to show a method for further analysis if necessary. The only use Eq. (5) in this paper means that the fraction of hard component is zero in low p_T region. In fact, it is right to exclude the contribution of hard component in low p_T region. As probability density functions, the integrals of Eqs. (3) and (4) [$f_0(p_T)$] are normalized to 1 respectively. Meanwhile, each component [$f_S(p_T)$ or $f_H(p_T)$] in Eqs. (3) and (4) is also normalized to 1 due to it being probability density function. When we compare $f_0(p_T)$ with experimental data, we have three main relations, $(1/2\pi p_T) d^2 N / dp_T dy = (1/2\pi p_T) N_0 f_0(p_T) / dy$, $d^2 N / dp_T dy = N_0 f_0(p_T) / dy$, and $dN / dp_T = N_0 f_0(p_T)$ according to different forms of cited data, where N and N_0 denote the particle number and normalization constant respectively. In some cases, N (N_0) can be replaced by the cross-section σ (normalization constant σ_0) if necessary.

From the above description, one can see that the method used in this paper is quite well known. Such kind of works of fitting the p_T spectra to thermal model or Hagedorn function have been done by many for decades. In particular, the low p_T hadrons produced in nuclear collisions are described by hydrodynamical models quite successfully [34, 35, 36]. However, we would like to point out that what we will report in the

following section is a more extensive application of the thermal model in high energy nuclear collisions at the RHIC and LHC. Meanwhile, the thermal model is more simpler in extracting the thermal parameters, while hydrodynamical models describe advantageously the evolution process of collision system [34, 35, 36]. Based on the thermal model, the centrality dependences of the kinetic freeze-out temperature T_0 , transverse flow velocity β_T , average transverse momentum $\langle p_T \rangle$, and initial temperature T_i for the emissions of identified particles, as well as the respective weighted averages are then obtained from systemizing the available experimental data. This systematic analysis on the centrality dependences of multiple parameters is a new attempt for us.

3 Results and discussion

3.1 Comparison with experimental data

Figure 1 presents the event centrality dependent double-differential p_T spectra, $(1/2\pi p_T)d^2N/dp_T dy$, of (a)(b) π^- , (c)(d) K^- , and (e)(f) \bar{p} produced in mid-pseudorapidity interval ($|\eta| < 0.35$) in (a)(c)(e) Au-Au and (b)(d)(f) d -Au collisions at $\sqrt{s_{NN}} = 200$ GeV at the RHIC, where y denotes rapidity and the mid-pseudorapidity interval is decided by the PHENIX experiment [16, 17] which we cited. The symbols represent the experimental data measured by the PHENIX Collaboration [16, 17]. The spectra in different centrality classes are scaled (multiplied) by different amounts marked in the panels, where the centrality classifications for Au-Au and d -Au collisions are different. The solid curves are our fitted results by using separately the blast-wave model with Boltzmann-Gibbs statistics, Eq. (5), where all the data points in the figure are used for fitting, though the low p_T range is satisfied primarily. The dashed curves are our simultaneous fit by the model, which will be discussed later. As a result, a special p_T range can be obtained, beyond which Eq. (5) does not work and $f_H(p_T)$ in Eq. (3) or (4) is needed. Corresponding to panels (a)–(f), the results of data/fit for the separate (simultaneous) fit are presented in panels (a')–(f') [(a'')–(f'')] respectively to monitor the departure of the separate (simultaneous) fit from data. In each fitting, the method of least squares is used in a special p_T range to obtain the best values of parameters. The values of free parameters (T_0 and β_T), normalization constant (N_0), χ^2 , and number of degree of freedom (ndof) are listed in Table 1, where the substantial event centralities and derived parameters which will be discussed later are listed together. In particular, N_0 satisfies $(1/2\pi p_T)d^2N/dp_T dy = (1/2\pi p_T)N_0 f_S(p_T)/dy$. One can see that the model results describe approximately the PHENIX data in special p_T ranges in high energy nuclear collisions at the RHIC.

In particular, the special p_T range is $0 \sim 2\text{--}3$ GeV/ c in peripheral collisions and $0 \sim 4.5$ GeV/ c or a little more in central collisions. This difference is caused by the fact that the multiple scatterings in peripheral collisions are less than those in central collisions due to less participant region in peripheral collisions, where the spectator in peripheral collisions has less influences. The special p_T range for strange particle is slightly narrower than that for non-strange particle. This difference is caused by the slightly less collision cross-section and then less frequency of multiple scatterings for strange particle K^- than for non-strange particles π^- and \bar{p} , which results in the special p_T range for strange particle to be slightly narrower. In addition, although Au-Au collisions have the same $\sqrt{s_{NN}}$ as d -Au collisions in Fig. 1, different sizes of participant regions for the two systems also affect the slopes of curves due to different frequencies of multiple scatterings. Usually, larger participant region and then more multiple scatterings result in more gentle curve. However, this influence is small due to the maximum size dependent effect [33].

Figure 2 is the same as Fig. 1, but it shows the results of (a) π^- , (c) K^- , and (e) \bar{p} produced in mid-rapidity interval $|y| < 0.5$ in Pb-Pb collisions at $\sqrt{s_{NN}} = 2.76$ TeV, and the results of (b) $\pi^+ + \pi^-$, (d) $K^+ + K^-$, and (f) $p + \bar{p}$ produced in $0 < y < 0.5$ in p -Pb collisions at $\sqrt{s_{NN}} = 5.02$ TeV, where the positive and negative particles in p -Pb collisions are not separated in experiments. The symbols represent the experimental data measured by the ALICE Collaboration [18, 19], where the spectra in Pb-Pb (or p -Pb) collisions are scaled by different amounts for different centrality classes shown in the panels and all the data points in the figure are used for fitting. Corresponding to panels (a)–(f), the results of data/fit for the separate (simultaneous) fit are presented in panels (a')–(f') [(a'')–(f'')] respectively. The related parameters are listed in Table 2, where the existent event centralities are listed together. One can see that the model results describe approximately the ALICE data in special p_T ranges in high energy nuclear collisions at the LHC. The special p_T range increases from $0 \sim 2\text{--}3$ GeV/ c to $0 \sim 4.5$ GeV/ c or a little more when the event centrality increases from periphery to center. This range for strange particle is slightly narrower than that for non-strange particle. The dependence of this range on energy is not obvious.

It should be noted that the uncertainties of free parameters T_0 and β_T are very small due to the strict restriction for the range of χ^2 . In fact, we restrict χ^2 so that $\chi^2_{\min} \leq \chi^2 \leq 1.05\chi^2_{\min}$, where χ^2_{\min} denotes the minimum- χ^2 which is obtained by the method of least squares and which changes for each fit (each particle in each centrality class). In the case of using weak restrictions, for example $\chi^2_{\min} \leq \chi^2 \leq 1.10\chi^2_{\min}$, large uncertainties will be obtained, which are not expected by us

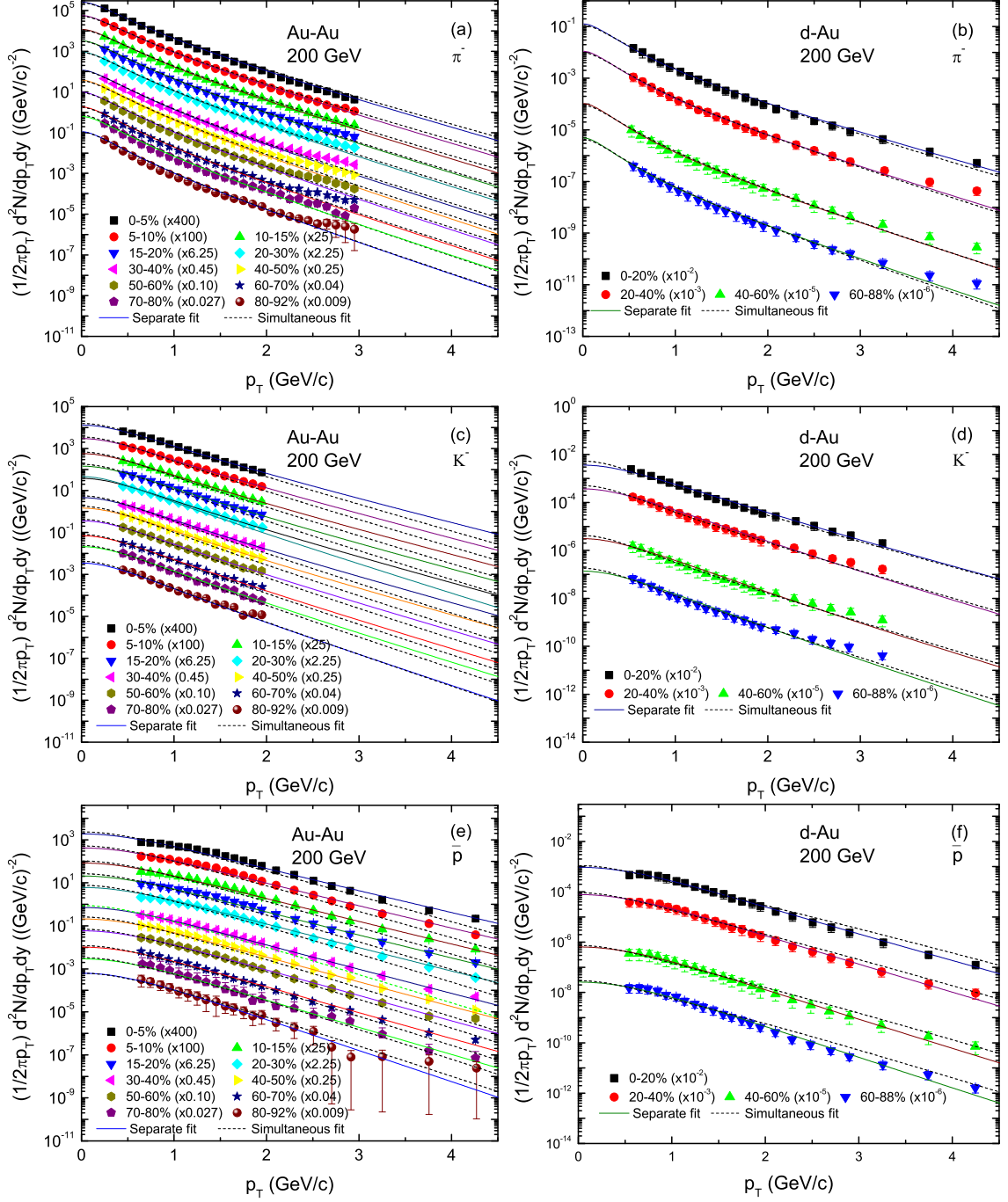


Fig. 1. Centrality dependent $(1/2\pi p_T)d^2N/dp_T dy$ of (a)(b) π^- , (c)(d) K^- , and (e)(f) \bar{p} produced in $|\eta| < 0.35$ in (a)(c)(e) Au-Au and (b)(d)(f) d-Au collisions at $\sqrt{s_{NN}} = 200$ GeV. The symbols represent the experimental data measured by the PHENIX Collaboration [16, 17]. The solid curves are our fitted results by using separately the blast-wave model with Boltzmann-Gibbs statistics, Eq. (5), while the dashed curves are those by using simultaneously the model. The spectra in different centrality classes are scaled by different amounts marked in the panels and all the data points in the figure are used for fitting.

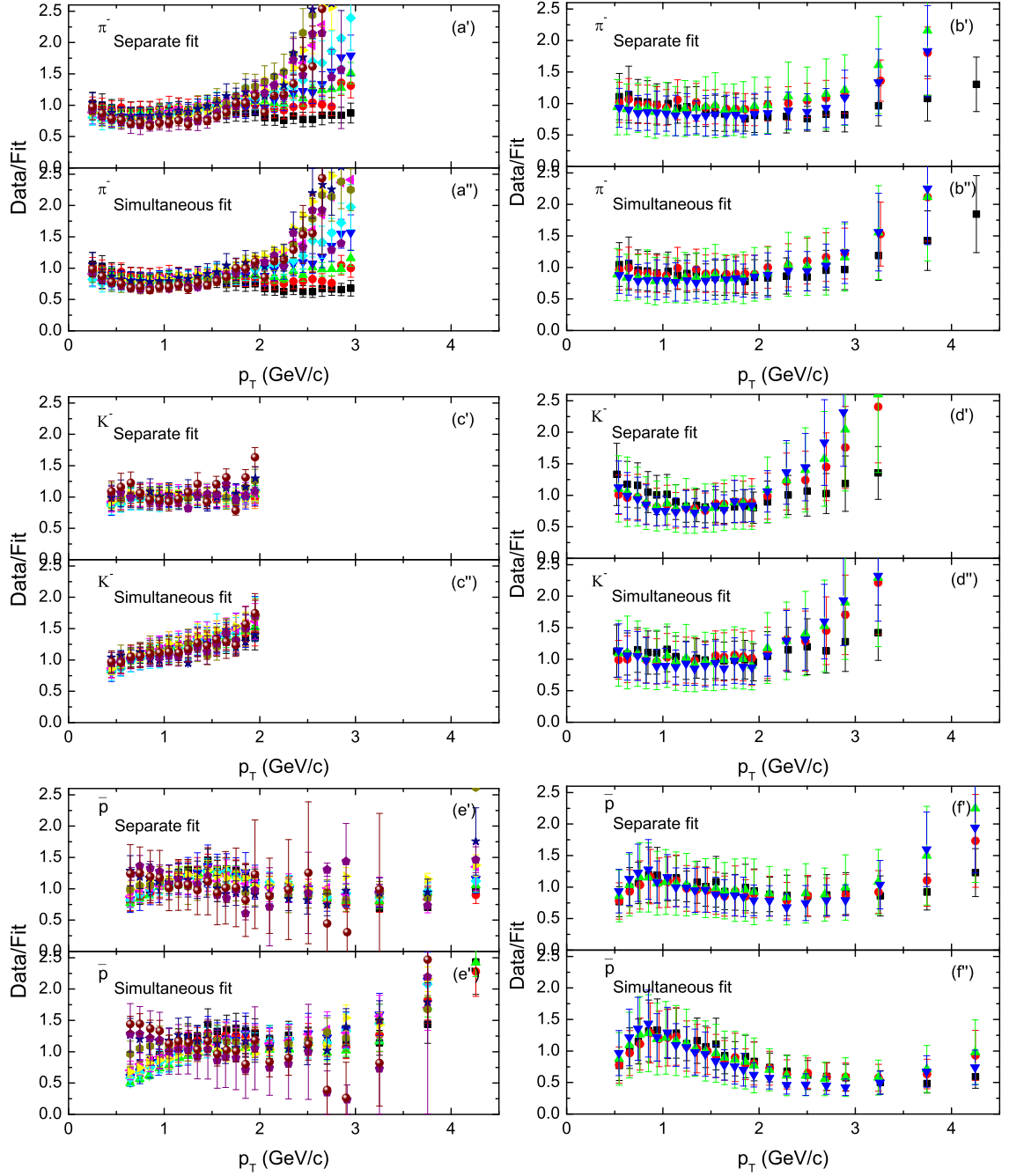


Fig. 1. Continued. Corresponding to panels (a)–(f), the results of data/fit for the separate (simultaneous) fit are presented in panels (a′)–(f′) [(a′′)–(f′′)] respectively to monitor the departure of the separate (simultaneous) fit from data. The error bars in the data/fit are calculated according to the error transfer formula in which only the statistical errors are considered.

due to inaccurate determination of parameters. In addition, Eq. (4) is not an ideal fitting function due to fewer free parameters being used in low p_T region, which renders small variable ranges of free parameters in limited selection. Contrarily, to give a better fit, Eq. (3) is more ideal due to more free parameters being used in low p_T region, which renders large variable ranges of free parameters by flexible selection. The limited selection in Eq. (4) restricts T_0 and β_T themselves.

In the fit in Figs. 1 and 2, because of only two free parameters being used, it is possibly coincidental if $\chi^2/\text{ndof} < 1$. Contrarily, the case of $\chi^2/\text{ndof} \gg 1$ is caused by the fact that the data points in high p_T region are included. Then, the two-component functions can be used if necessary. This paper is focused on the extraction of centrality dependence of T_0 and β_T in nuclear collisions at the top RHIC and LHC energies. In fact, we do not need to consider the data points in

Table 1. Values of T_0 , β_T , $\langle p_T \rangle$, T_i , N_0 , χ^2 , and ndof corresponding to the solid curves in Fig. 1.

| Figure | Particle | Centrality | T_0 (GeV) | β_T (c) | $\langle p_T \rangle$ (GeV/c) | T_i (GeV) | N_0 | χ^2 | ndof |
|-----------------------------------|-----------|-------------------|-------------------|-------------------|-------------------------------|-------------------|-------------------|-----------------|------|
| Fig. 1 Au-Au 200 GeV | π^- | 0-5% | 0.140 ± 0.004 | 0.368 ± 0.004 | 0.467 ± 0.023 | 0.412 ± 0.021 | 46.00 ± 2.50 | 34 | 25 |
| | | 5-10% | 0.138 ± 0.005 | 0.365 ± 0.005 | 0.458 ± 0.022 | 0.403 ± 0.021 | 39.00 ± 2.00 | 9 | 25 |
| | | 10-15% | 0.136 ± 0.003 | 0.364 ± 0.005 | 0.451 ± 0.022 | 0.397 ± 0.020 | 32.00 ± 1.40 | 57 | 25 |
| | | 15-20% | 0.132 ± 0.004 | 0.366 ± 0.006 | 0.440 ± 0.022 | 0.388 ± 0.019 | 33.60 ± 2.00 | 39 | 25 |
| | | 20-30% | 0.130 ± 0.004 | 0.364 ± 0.004 | 0.433 ± 0.022 | 0.381 ± 0.019 | 25.30 ± 2.00 | 79 | 25 |
| | | 30-40% | 0.128 ± 0.004 | 0.365 ± 0.006 | 0.428 ± 0.021 | 0.376 ± 0.019 | 18.00 ± 0.60 | 111 | 25 |
| | | 40-50% | 0.127 ± 0.003 | 0.360 ± 0.005 | 0.421 ± 0.022 | 0.369 ± 0.018 | 8.95 ± 0.44 | 286 | 25 |
| | | 50-60% | 0.126 ± 0.003 | 0.365 ± 0.004 | 0.420 ± 0.021 | 0.371 ± 0.019 | 5.80 ± 0.27 | 111 | 25 |
| | | 60-70% | 0.125 ± 0.005 | 0.365 ± 0.004 | 0.419 ± 0.020 | 0.368 ± 0.018 | 2.70 ± 0.30 | 91 | 25 |
| | 70-80% | 0.123 ± 0.004 | 0.364 ± 0.006 | 0.412 ± 0.021 | 0.362 ± 0.018 | 1.40 ± 0.07 | 92 | 25 | |
| | 80-92% | 0.120 ± 0.003 | 0.367 ± 0.005 | 0.406 ± 0.020 | 0.357 ± 0.018 | 0.69 ± 0.02 | 293 | 25 | |
| | K^- | 0-5% | 0.180 ± 0.005 | 0.346 ± 0.006 | 0.702 ± 0.035 | 0.599 ± 0.030 | 6.85 ± 0.25 | 1 | 13 |
| | | 5-10% | 0.176 ± 0.006 | 0.345 ± 0.008 | 0.688 ± 0.034 | 0.587 ± 0.029 | 6.02 ± 0.27 | 1 | 13 |
| | | 10-15% | 0.174 ± 0.006 | 0.344 ± 0.006 | 0.682 ± 0.034 | 0.581 ± 0.029 | 4.54 ± 0.23 | 5 | 13 |
| | | 15-20% | 0.172 ± 0.004 | 0.340 ± 0.006 | 0.671 ± 0.034 | 0.571 ± 0.029 | 4.48 ± 0.24 | 1 | 13 |
| | | 20-30% | 0.170 ± 0.007 | 0.338 ± 0.007 | 0.663 ± 0.033 | 0.564 ± 0.028 | 3.20 ± 0.27 | 2 | 13 |
| | | 30-40% | 0.169 ± 0.004 | 0.337 ± 0.005 | 0.659 ± 0.032 | 0.560 ± 0.028 | 1.92 ± 0.10 | 1 | 13 |
| | | 40-50% | 0.167 ± 0.005 | 0.335 ± 0.006 | 0.651 ± 0.033 | 0.553 ± 0.028 | 1.07 ± 0.07 | 2 | 13 |
| | | 50-60% | 0.164 ± 0.004 | 0.330 ± 0.007 | 0.637 ± 0.032 | 0.540 ± 0.027 | 0.64 ± 0.06 | 3 | 13 |
| | | 60-70% | 0.160 ± 0.004 | 0.327 ± 0.005 | 0.623 ± 0.031 | 0.528 ± 0.026 | 0.30 ± 0.03 | 4 | 13 |
| | 70-80% | 0.156 ± 0.004 | 0.326 ± 0.008 | 0.611 ± 0.031 | 0.517 ± 0.026 | 0.13 ± 0.02 | 49 | 13 | |
| | 80-92% | 0.150 ± 0.006 | 0.317 ± 0.007 | 0.585 ± 0.029 | 0.494 ± 0.025 | 0.06 ± 0.03 | 49 | 13 | |
| | \bar{p} | 0-5% | 0.208 ± 0.006 | 0.333 ± 0.005 | 0.939 ± 0.047 | 0.786 ± 0.039 | 1.97 ± 0.10 | 36 | 19 |
| | | 5-10% | 0.206 ± 0.005 | 0.326 ± 0.004 | 0.926 ± 0.046 | 0.775 ± 0.039 | 1.71 ± 0.11 | 25 | 19 |
| 10-15% | | 0.204 ± 0.005 | 0.325 ± 0.007 | 0.919 ± 0.046 | 0.769 ± 0.038 | 1.34 ± 0.04 | 63 | 19 | |
| 15-20% | | 0.203 ± 0.004 | 0.322 ± 0.004 | 0.912 ± 0.046 | 0.762 ± 0.038 | 0.13 ± 0.06 | 7 | 19 | |
| 20-30% | | 0.200 ± 0.005 | 0.319 ± 0.004 | 0.898 ± 0.045 | 0.751 ± 0.038 | 0.13 ± 0.11 | 22 | 19 | |
| 30-40% | | 0.198 ± 0.004 | 0.312 ± 0.004 | 0.881 ± 0.044 | 0.735 ± 0.037 | 0.60 ± 0.02 | 8 | 19 | |
| 40-50% | | 0.196 ± 0.006 | 0.308 ± 0.003 | 0.870 ± 0.044 | 0.725 ± 0.036 | 0.31 ± 0.03 | 22 | 19 | |
| 50-60% | | 0.191 ± 0.003 | 0.305 ± 0.003 | 0.852 ± 0.043 | 0.710 ± 0.036 | 0.21 ± 0.02 | 33 | 19 | |
| 60-70% | | 0.188 ± 0.004 | 0.304 ± 0.004 | 0.843 ± 0.042 | 0.702 ± 0.035 | 0.090 ± 0.010 | 35 | 19 | |
| 70-80% | | 0.184 ± 0.003 | 0.294 ± 0.003 | 0.818 ± 0.042 | 0.679 ± 0.034 | 0.036 ± 0.002 | 68 | 19 | |
| 80-92% | | 0.162 ± 0.006 | 0.285 ± 0.005 | 0.749 ± 0.038 | 0.620 ± 0.031 | 0.020 ± 0.002 | 194 | 19 | |
| Fig. 1 <i>d</i> -Au 200 GeV | | π^- | 0-20% | 0.120 ± 0.003 | 0.443 ± 0.003 | 0.504 ± 0.033 | 0.464 ± 0.023 | 0.86 ± 0.04 | 10 |
| | 20-40% | | 0.117 ± 0.004 | 0.436 ± 0.003 | 0.481 ± 0.022 | 0.440 ± 0.022 | 0.70 ± 0.08 | 10 | 21 |
| | 40-60% | | 0.112 ± 0.004 | 0.435 ± 0.004 | 0.462 ± 0.023 | 0.422 ± 0.021 | 0.62 ± 0.06 | 7 | 21 |
| | 60-88% | | 0.109 ± 0.003 | 0.432 ± 0.004 | 0.447 ± 0.022 | 0.406 ± 0.020 | 0.28 ± 0.02 | 15 | 21 |
| | K^- | 0-20% | 0.239 ± 0.006 | 0.254 ± 0.005 | 0.752 ± 0.038 | 0.635 ± 0.032 | 0.100 ± 0.010 | 8 | 18 |
| | | 20-40% | 0.235 ± 0.004 | 0.250 ± 0.005 | 0.738 ± 0.037 | 0.622 ± 0.031 | 0.090 ± 0.005 | 9 | 18 |
| | | 40-60% | 0.230 ± 0.005 | 0.248 ± 0.003 | 0.724 ± 0.036 | 0.610 ± 0.031 | 0.073 ± 0.005 | 6 | 18 |
| | | 60-88% | 0.218 ± 0.004 | 0.247 ± 0.006 | 0.694 ± 0.035 | 0.584 ± 0.029 | 0.030 ± 0.003 | 18 | 18 |
| | \bar{p} | 0-20% | 0.262 ± 0.004 | 0.238 ± 0.006 | 0.935 ± 0.047 | 0.777 ± 0.039 | 0.042 ± 0.004 | 6 | 21 |
| | | 20-40% | 0.260 ± 0.005 | 0.230 ± 0.005 | 0.922 ± 0.046 | 0.765 ± 0.038 | 0.033 ± 0.002 | 6 | 21 |
| | | 40-60% | 0.250 ± 0.006 | 0.228 ± 0.005 | 0.896 ± 0.045 | 0.743 ± 0.037 | 0.026 ± 0.003 | 4 | 21 |
| | | 60-88% | 0.245 ± 0.004 | 0.215 ± 0.005 | 0.870 ± 0.044 | 0.721 ± 0.036 | 0.010 ± 0.001 | 14 | 21 |

high p_T region. On one hand, these data points have zero contribution due to their non-thermal processes, which should be excluded. On the other hand, these data points have less contributions due to their small amounts, which can be neglected. In the calculation of χ^2/ndof , we have included these data points, which causes $\chi^2/\text{ndof} \gg 1$.

3.2 Trend of parameters

To study the dependences of T_0 and β_T on the event centrality, Figures 3 and 4 show the correlations between T_0 and C as well as β_T and C respectively, where C denotes the event centrality percentage in which 0% centrality is the most central collisions and 100% centrality is the most peripheral collisions. Different symbols represent different parameter values listed in Tables 1 and 2. In particular, the averages, $\langle T_0 \rangle$ ($\langle \beta_T \rangle$), of T_0 (β_T) weighted over yields of different particles are shown in Fig. 3 (4) by the open circles. It can be seen that, T_0

and β_T increase slightly in some cases or almost do not change in other cases with the increase of event centrality from peripheral to central collisions. This difference should be studied in the future. In particular, for T_0 from K and p spectra there is slight centrality dependence, while for T_0 from π spectra at the LHC there is no obvious centrality dependence. Except K and p in Au-Au collisions at 200 GeV and p in p -Pb collisions at 5.02 TeV, there is no dependence of the parameter β_T on centrality. With the increase of particle mass, T_0 increases while β_T decreases obviously. In most cases, T_0 and β_T in Pb-Pb (p -Pb) collisions at the LHC are comparable with those in Au-Au (d -Au) collisions at the RHIC within errors. At the same time, T_0 and β_T in Au-Au (Pb-Pb) collisions are comparable with those in d -Au (p -Pb) collisions within errors. In short, T_0 and β_T do not decrease in general with the increase of event centrality, collision energy, and projectile size (in the case of the same target nucleus) within errors, and T_0 (β_T) increases (decreases) obviously with

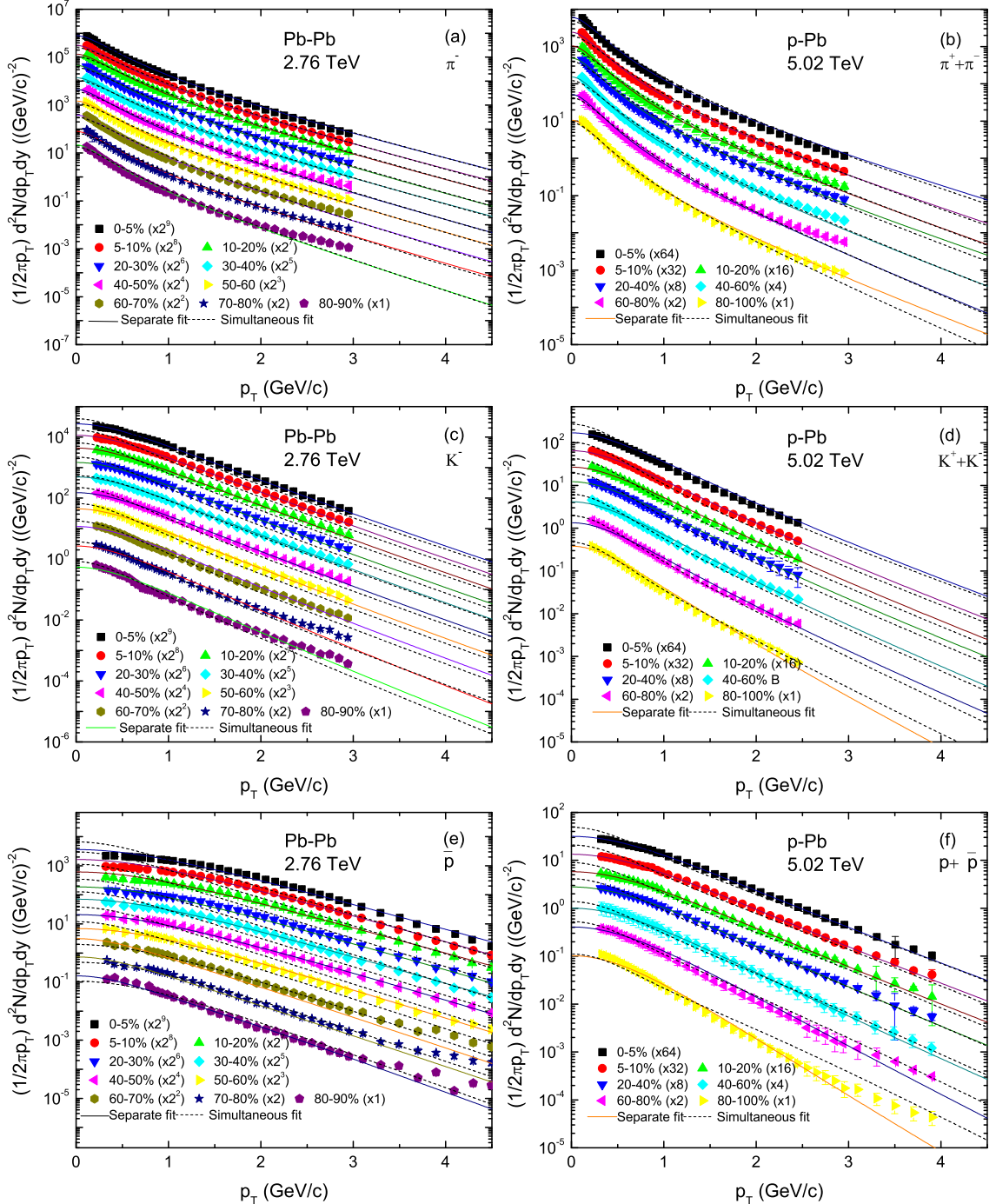


Fig. 2. Same as Fig. 1, but for the spectra of (a) π^- , (c) K^- , and (e) \bar{p} produced in $|y| < 0.5$ in Pb-Pb collisions at $\sqrt{s_{NN}} = 2.76$ TeV, and the spectra of (b) $\pi^+ + \pi^-$, (d) $K^+ + K^-$, and (f) $p + \bar{p}$ produced in $0 < y < 0.5$ in p -Pb collisions at $\sqrt{s_{NN}} = 5.02$ TeV. The symbols represent the experimental data measured by the ALICE Collaboration [18, 19], where the spectra in different centrality classes are scaled by different amounts shown in the panels and all the data points in the figure are used for fitting.

the increase of particle mass. The mass dependent T_0 and β_T is a reflection of the scenario of multiple kinetic freeze-out [22]. According to the hydrodynamical behavior [39], the massive particles are left over early due to small β_T . Meanwhile, early emission results in high T_0 .

We would like to point out that although we fit the three spectra of identified particle species individually in Figs. 1 and 2 by the solid curves, the average parameters weighted by particle yields N_0 in Tables 1 and 2 should be used for the three particles simultaneously by the dashed curves. Figures 3 and 4 show that the aver-

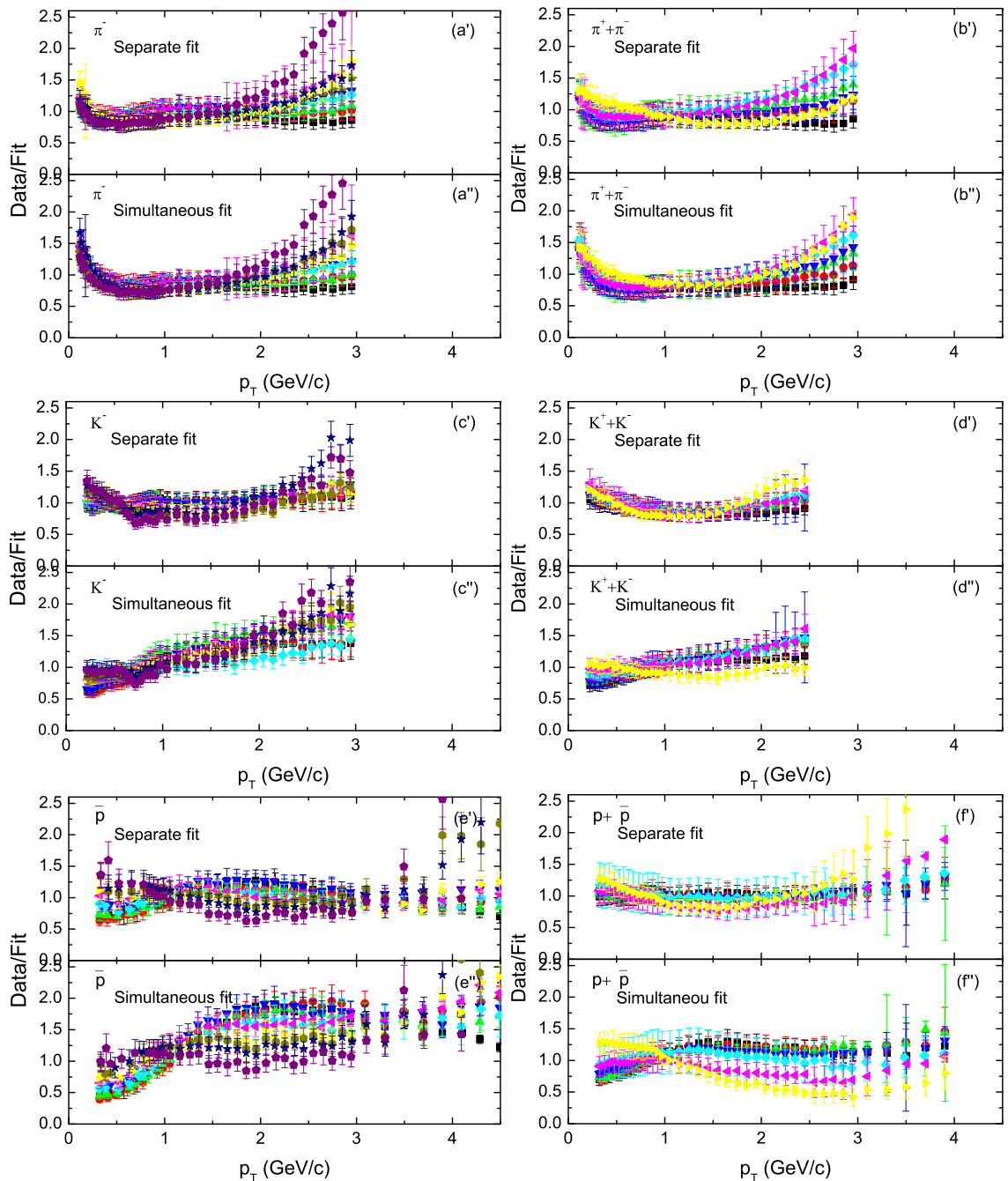


Fig. 2. Continued. Corresponding to panels (a)–(f), the results of data/fit for the separate (simultaneous) fit are presented in panels (a′)–(f′) [(a′′)–(f′′)] respectively to monitor the departure of the separate (simultaneous) fit from data. The error bars in the data/fit are calculated according to the error transfer formula in which only the statistical errors are considered.

age parameters weighted by particle yields are closer to those for pions due to the fact that the yield of pions is the most at the considered energy. We notice that the average T_0 over all particles in given centrality is close to or does not exceed the chemical freeze-out temperature in general. In addition, when we apply the weighted average parameters for kaons and protons, we obtain relative large χ^2 . The dashed curves in Figs. 1 and 2 show that both the simultaneous fits at the RHIC and LHC

are approximately and similarly successful. It should be noted that the multiplicity weighted mean parameters are identified with a single $\langle T_0 \rangle$ and $\langle \beta_T \rangle$ which is obtained by the fit of all particles in a given centrality class. These mean parameters may be different from T_0 and β_T used in Refs. [2, 18] due to different restricted conditions. These restrictions include the particle-dependent or independent p_T range, unfixed or fixed flow profile (n_0), and large or small β_T change. The present work

Table 2. Values of T_0 , β_T , $\langle p_T \rangle$, T_i , N_0 , χ^2 , and ndof corresponding to the solid curves in Fig. 2.

| Figure | Particle | Centrality | T_0 (GeV) | β_T (c) | $\langle p_T \rangle$ (GeV/c) | T_i (GeV) | N_0 | χ^2 | ndof | |
|-----------------------------|-------------------|-------------------|-------------------|-------------------|-------------------------------|-------------------|--------------------|-----------------|------|----|
| Fig. 2 Pb-Pb 2.76 TeV | π^- | 0-5% | 0.135 ± 0.003 | 0.430 ± 0.003 | 0.532 ± 0.027 | 0.485 ± 0.024 | 123.39 ± 1.95 | 31 | 38 | |
| | | 5-10% | 0.134 ± 0.004 | 0.429 ± 0.004 | 0.526 ± 0.003 | 0.479 ± 0.024 | 105.34 ± 11.72 | 8 | 38 | |
| | | 10-20% | 0.132 ± 0.004 | 0.428 ± 0.005 | 0.518 ± 0.026 | 0.471 ± 0.024 | 78.36 ± 7.81 | 15 | 38 | |
| | | 20-30% | 0.129 ± 0.003 | 0.427 ± 0.006 | 0.506 ± 0.025 | 0.459 ± 0.023 | 51.56 ± 4.69 | 28 | 38 | |
| | | 30-40% | 0.131 ± 0.005 | 0.428 ± 0.005 | 0.514 ± 0.026 | 0.468 ± 0.023 | 34.87 ± 3.11 | 20 | 38 | |
| | | 40-50% | 0.127 ± 0.003 | 0.426 ± 0.004 | 0.497 ± 0.025 | 0.451 ± 0.023 | 20.23 ± 2.50 | 20 | 38 | |
| | | 50-60% | 0.124 ± 0.003 | 0.428 ± 0.004 | 0.490 ± 0.025 | 0.445 ± 0.022 | 12.02 ± 1.25 | 67 | 38 | |
| | | 60-70% | 0.123 ± 0.004 | 0.426 ± 0.005 | 0.483 ± 0.024 | 0.438 ± 0.022 | 6.43 ± 0.04 | 72 | 38 | |
| | | 70-80% | 0.126 ± 0.004 | 0.424 ± 0.005 | 0.490 ± 0.025 | 0.444 ± 0.022 | 2.75 ± 0.30 | 83 | 38 | |
| | 80-90% | 0.108 ± 0.004 | 0.428 ± 0.006 | 0.435 ± 0.022 | 0.395 ± 0.020 | 1.20 ± 0.20 | 165 | 38 | | |
| | K^- | 0-5% | 0.289 ± 0.005 | 0.228 ± 0.004 | 0.851 ± 0.043 | 0.717 ± 0.036 | 16.80 ± 0.59 | 4 | 33 | |
| | | 5-10% | 0.287 ± 0.006 | 0.227 ± 0.007 | 0.845 ± 0.042 | 0.713 ± 0.036 | 14.67 ± 1.17 | 6 | 33 | |
| | | 10-20% | 0.284 ± 0.005 | 0.225 ± 0.006 | 0.836 ± 0.042 | 0.705 ± 0.035 | 10.55 ± 0.78 | 11 | 33 | |
| | | 20-30% | 0.282 ± 0.004 | 0.227 ± 0.005 | 0.833 ± 0.042 | 0.702 ± 0.035 | 7.03 ± 0.63 | 17 | 33 | |
| | | 30-40% | 0.281 ± 0.007 | 0.225 ± 0.005 | 0.829 ± 0.041 | 0.699 ± 0.035 | 4.69 ± 0.47 | 14 | 33 | |
| | | 40-50% | 0.279 ± 0.006 | 0.222 ± 0.008 | 0.821 ± 0.041 | 0.692 ± 0.035 | 2.81 ± 0.13 | 19 | 33 | |
| | | 50-60% | 0.275 ± 0.005 | 0.219 ± 0.008 | 0.810 ± 0.041 | 0.682 ± 0.034 | 1.63 ± 0.13 | 41 | 33 | |
| | | 60-70% | 0.271 ± 0.006 | 0.217 ± 0.009 | 0.799 ± 0.040 | 0.672 ± 0.034 | 0.84 ± 0.10 | 74 | 33 | |
| | | 70-80% | 0.255 ± 0.007 | 0.215 ± 0.010 | 0.759 ± 0.038 | 0.638 ± 0.032 | 0.37 ± 0.20 | 105 | 33 | |
| | 80-90% | 0.254 ± 0.007 | 0.209 ± 0.012 | 0.752 ± 0.038 | 0.632 ± 0.032 | 0.14 ± 0.01 | 179 | 33 | | |
| | \bar{p} | 0-5% | 0.443 ± 0.005 | 0.098 ± 0.008 | 1.234 ± 0.062 | 1.020 ± 0.051 | 5.27 ± 0.39 | 81 | 34 | |
| | | 5-10% | 0.440 ± 0.004 | 0.050 ± 0.007 | 1.211 ± 0.061 | 1.000 ± 0.050 | 4.69 ± 0.35 | 98 | 34 | |
| | | 10-20% | 0.438 ± 0.004 | 0.090 ± 0.007 | 1.220 ± 0.061 | 1.008 ± 0.050 | 3.52 ± 0.23 | 61 | 34 | |
| | | 20-30% | 0.435 ± 0.004 | 0.060 ± 0.008 | 1.203 ± 0.060 | 0.994 ± 0.050 | 2.11 ± 0.16 | 45 | 34 | |
| 30-40% | | 0.430 ± 0.005 | 0.055 ± 0.013 | 1.191 ± 0.060 | 0.984 ± 0.049 | 1.56 ± 0.19 | 26 | 34 | | |
| 40-50% | | 0.427 ± 0.004 | 0.026 ± 0.016 | 1.180 ± 0.059 | 0.974 ± 0.049 | 0.90 ± 0.03 | 16 | 34 | | |
| 50-60% | | 0.405 ± 0.003 | 0.060 ± 0.012 | 1.139 ± 0.057 | 0.940 ± 0.047 | 0.56 ± 0.02 | 48 | 34 | | |
| 60-70% | | 0.378 ± 0.004 | 0.046 ± 0.012 | 1.076 ± 0.054 | 0.888 ± 0.044 | 0.29 ± 0.01 | 53 | 34 | | |
| 70-80% | | 0.362 ± 0.004 | 0.089 ± 0.004 | 1.054 ± 0.053 | 0.870 ± 0.044 | 0.14 ± 0.02 | 72 | 34 | | |
| 80-90% | 0.340 ± 0.005 | 0.080 ± 0.009 | 1.001 ± 0.050 | 0.826 ± 0.041 | 0.055 ± 0.004 | 161 | 34 | | | |
| Fig. 2 p-Pb 5.02 TeV | $\pi^+ + \pi^-$ | 0-5% | 0.119 ± 0.006 | 0.469 ± 0.005 | 0.576 ± 0.029 | 0.546 ± 0.027 | 7.23 ± 0.47 | 31 | 38 | |
| | | 5-10% | 0.116 ± 0.006 | 0.465 ± 0.005 | 0.549 ± 0.027 | 0.518 ± 0.026 | 5.35 ± 0.01 | 11 | 38 | |
| | | 10-20% | 0.113 ± 0.007 | 0.462 ± 0.006 | 0.528 ± 0.026 | 0.495 ± 0.025 | 4.38 ± 0.01 | 14 | 38 | |
| | | 20-40% | 0.112 ± 0.005 | 0.460 ± 0.004 | 0.530 ± 0.027 | 0.499 ± 0.025 | 4.06 ± 0.13 | 26 | 38 | |
| | | 40-60% | 0.110 ± 0.004 | 0.457 ± 0.005 | 0.502 ± 0.025 | 0.468 ± 0.023 | 2.40 ± 0.25 | 85 | 38 | |
| | | 60-80% | 0.107 ± 0.005 | 0.453 ± 0.004 | 0.480 ± 0.024 | 0.445 ± 0.022 | 1.55 ± 0.06 | 44 | 38 | |
| | | 80-100% | 0.100 ± 0.001 | 0.463 ± 0.001 | 0.480 ± 0.024 | 0.450 ± 0.023 | 0.60 ± 0.05 | 291 | 38 | |
| | | $K^+ + K^-$ | 0-5% | 0.293 ± 0.005 | 0.313 ± 0.005 | 0.951 ± 0.048 | 0.812 ± 0.041 | 0.98 ± 0.05 | 49 | 28 |
| | | | 5-10% | 0.285 ± 0.003 | 0.310 ± 0.004 | 0.926 ± 0.046 | 0.791 ± 0.040 | 0.71 ± 0.02 | 13 | 28 |
| | 10-20% | | 0.279 ± 0.005 | 0.307 ± 0.006 | 0.907 ± 0.045 | 0.774 ± 0.039 | 0.57 ± 0.04 | 57 | 28 | |
| | 20-40% | | 0.270 ± 0.006 | 0.312 ± 0.007 | 0.891 ± 0.045 | 0.760 ± 0.038 | 0.50 ± 0.04 | 12 | 28 | |
| | 40-60% | | 0.255 ± 0.004 | 0.310 ± 0.005 | 0.850 ± 0.043 | 0.725 ± 0.036 | 0.31 ± 0.03 | 70 | 28 | |
| | 60-80% | | 0.232 ± 0.004 | 0.329 ± 0.005 | 0.815 ± 0.041 | 0.697 ± 0.035 | 0.19 ± 0.01 | 24 | 28 | |
| | 80-100% | | 0.200 ± 0.005 | 0.309 ± 0.006 | 0.707 ± 0.035 | 0.600 ± 0.030 | 0.083 ± 0.007 | 77 | 28 | |
| | $p + \bar{p}$ | | 0-5% | 0.355 ± 0.005 | 0.293 ± 0.004 | 1.229 ± 0.061 | 1.026 ± 0.051 | 0.34 ± 0.02 | 5 | 36 |
| | | | 5-10% | 0.350 ± 0.006 | 0.290 ± 0.005 | 1.213 ± 0.061 | 1.012 ± 0.051 | 0.28 ± 0.01 | 5 | 36 |
| | | 10-20% | 0.340 ± 0.006 | 0.289 ± 0.006 | 1.188 ± 0.059 | 0.992 ± 0.050 | 0.24 ± 0.01 | 14 | 36 | |
| | | 20-40% | 0.325 ± 0.005 | 0.282 ± 0.007 | 1.143 ± 0.057 | 0.954 ± 0.048 | 0.20 ± 0.01 | 19 | 36 | |
| | | 40-60% | 0.320 ± 0.006 | 0.276 ± 0.005 | 1.075 ± 0.054 | 0.897 ± 0.045 | 0.14 ± 0.01 | 35 | 36 | |
| | | 60-80% | 0.295 ± 0.006 | 0.227 ± 0.007 | 1.001 ± 0.050 | 0.832 ± 0.042 | 0.10 ± 0.01 | 26 | 36 | |
| | | 80-100% | 0.240 ± 0.006 | 0.238 ± 0.006 | 0.883 ± 0.044 | 0.732 ± 0.037 | 0.040 ± 0.004 | 50 | 36 | |

uses the restrictions of particle-independent p_T range, fixed flow profile ($n_0 = 2$ as used in ref. [1]), and small β_T change, which contains less free parameters in the analysis and larger flow effect in peripheral collisions.

If simultaneous fit has more credibility in general, the different values of freeze-out parameters for individual particles imply a multiple kinetic freeze-out scenario [10, 22, 37, 38] in terms of detailed analysis. For particles in collisions with given centrality, the higher the T_0 is, the earlier the emission of the particles is. As one of constituents in projectile and target participants, some protons are leading protons which are existed in the initial state of collisions and they are emitted much earlier than pions due to their existence before thermalization. Even if other protons formed in the collisions are emitted simultaneously with pions, on

average, protons are emitted earlier than pions. Generally, leading protons emitted earlier than pions appear in the forward/backward rapidity region, while protons emitted simultaneously with pions appear in the whole rapidity region as pions. At the LHC, the large difference in T_0 for different particles renders naturally large difference in emission time. On the other hand, the mass-dependent multiple scenario “shows massive particles coming out of the system earlier in time with smaller radial flow velocities, which is hydrodynamic behavior” [39]. This earlier freeze-out for massive particles appear due to the fact that they are left behind in the system process due to low β_T and large m_0 , but not high T_0 . For collisions with different centralities, the higher the T_0 is, the higher the excitation degree is. Finally, T_0 is a result of competition between excitation degree

and emission time.

In addition, we have used the specific profile for the transverse flow velocity which is also used in the original blast-wave model with Boltzmann-Gibbs statistics [1, 2, 3], though the profile is sensitive to the fit for transverse momentum spectra as explored e.g. in refs. [18, 40]. This sensitive profile affects only the absolute sizes of T_0 (β_T) for emissions of individual particles, but not the relative sizes. In other words, this sensitive profile does not affect our conclusions on multiple kinetic freeze-out scenario [10, 22, 37, 38] in terms of detailed analysis and more credible simultaneous fit in general. It does not affect the trend on centrality dependence of T_0 (β_T) too, which are discussed in Figs. 3 and 4. Therefore, we would like not to use other specific profiles in the present work.

In the fit process for Figs. 1 and 2, the parameters T_0 and β_T are correlated. In some cases, a larger T_0 and a smaller β_T can lead to a similar result by using a smaller T_0 and a larger β_T due to the influence of p_T range and n_0 if changeable. To reduce the effect of correlation, we analyze the mean p_T ($\langle p_T \rangle$) and the root-mean-square p_T ($\sqrt{\langle p_T^2 \rangle}$) over $\sqrt{2}$ ($\sqrt{\langle p_T^2 \rangle}/2$) in Figs. 5 and 6 respectively, which are calculated from the fit function over a given p_T range of 0–4.5 GeV/ c , where T_i represents $\sqrt{\langle p_T^2 \rangle}/2$ to denote the initial temperature of the interacting system according to the color string percolation model [41, 42, 43]. In particular, the weighted averages, $\overline{\langle p_T \rangle}$ ($\langle T_i \rangle$), of $\langle p_T \rangle$ (T_i) over different particles are shown in Fig. 5 (6) by the open circles, which are calculated from the fit function and weighted by yields of different particles. One can see that $\langle p_T \rangle$ and T_i increase with the increases of event centrality, collision energy, and particle mass. With the increase of projectile size in the case of using the same target nucleus, $\langle p_T \rangle$ and T_i do not change obviously.

It should be noted that we have used T_i according to refs. [41, 42, 43]. When we use $\langle T_i \rangle$, it is independent of specie of the measured particle. It is noteworthy to measure T_i for the emission of different particles in order to obtain $\langle T_i \rangle$. Although T_i is directly equal to $\sqrt{\langle p_T^2 \rangle}/2$ which can be obtained from p_T spectra, one should obtain T_i as usual to see its trend. Our discussions on T_i and $\langle T_i \rangle$ are useful to understand the excitation degree of the system in the initial state. Meanwhile, we may compare T_i and $\langle T_i \rangle$ with T_0 and $\langle T_0 \rangle$ to see the decrease of temperature in the system evolution.

Generally, large T_0 (β_T) renders wide p_T spectrum and then large $\langle p_T \rangle$. In central collisions, we have obtained larger T_0 (β_T) and larger $\langle p_T \rangle$ than those in peripheral collisions. The normalizations (N_0) listed in Tables 1 and 2 are in fact the (pseudo)rapidity density ($dN/d\eta$ or dN/dy) of identified particles at mid-rapidity. One can see a decrease trend from central to peripheral collisions. This trend is similar to that of T_0 (β_T)

and $\langle p_T \rangle$, but with different slopes. This trend renders more energy deposition and more violent impact (larger squeeze) in central collisions, which results in higher excitation (larger T_0) and quicker expansion (larger β_T). Naturally, we can obtain larger $\langle p_T \rangle$, T_i , and $dN/d\eta$ in central collisions comparing with those in peripheral collisions. Although the parameters T_0 , β_T , and T_i are extracted from a model, they are in fact based on the fit to experimental data. In particular, T_i can be regarded as an experimental result. It is regretful that there is no direct experimental values on T_0 and β_T .

It should be noted that T_i used in refs. [33, 37, 38, 40, 41, 42, 43] depends on $\sqrt{\langle p_T^2 \rangle}/2$ itself, but not models. If we use the data directly, we should also obtain T_i . It is suitable that T_i is used in the present work. In addition, T_0 obtained from proton spectra in Pb-Pb collisions at the LHC comes out larger than 300 MeV, in central Pb-Pb collisions this is even 443 MeV. This way is above the hadronization temperature, which seems hardly to be understandable. In fact, the weighted average temperatures $\langle T_0 \rangle$ are the kinetic freeze-out temperatures of the system. The hadronization temperature is mainly determined by that from pion spectrum due to the fact that the yield of pions is the largest one among those of the produced particles. In our opinion, as the kinetic freeze-out temperatures, the values of $\langle T_0 \rangle$ obtained in the present work are normal. As a statistical quantity and a reflection of mean thermal motion, $\langle T_0 \rangle$ can be naturally used in our study.

We would like to point out that, although Eq. (5) for the blast-wave model is obtained by assuming that the system is in local thermodynamic equilibrium, and therefore, it assumes a single T_0 and β_T , the single T_0 and β_T can be $\langle T_0 \rangle$ and $\langle \beta_T \rangle$ respectively. Generally, $\langle T_0 \rangle$ ($\langle \beta_T \rangle$, $\overline{\langle p_T \rangle}$, or $\langle T_i \rangle$) is mainly determined by that emitting pions due to the largest yield of pions at the top RHIC and LHC energies. Meanwhile, $\langle T_0 \rangle$ ($\langle \beta_T \rangle$) reflects approximately a combined fit to different particle species. Indeed, statistical fluctuations in the data in different collisions with different centralities produce fluctuations in the fitted parameters.

The reason that T_0 or β_T does not decrease with the increase of event centrality and collision energy renders that the violent degree of thermal excitation and collective behavior at the stage of kinetic freeze-out in interacting system does not decrease with increase of event centrality and collision energy. This results in faster or the same thermal motion and collective expansion which are reflected by T_0 and β_T respectively. In addition, in peripheral collisions, a larger fraction in high p_T region is observed due to larger cascade scattering happening in spectator nucleons and appreciable contribution from the hard component, and that results in the departure of statistical law from the thermal model in high p_T region, which results in the appearance of special p_T

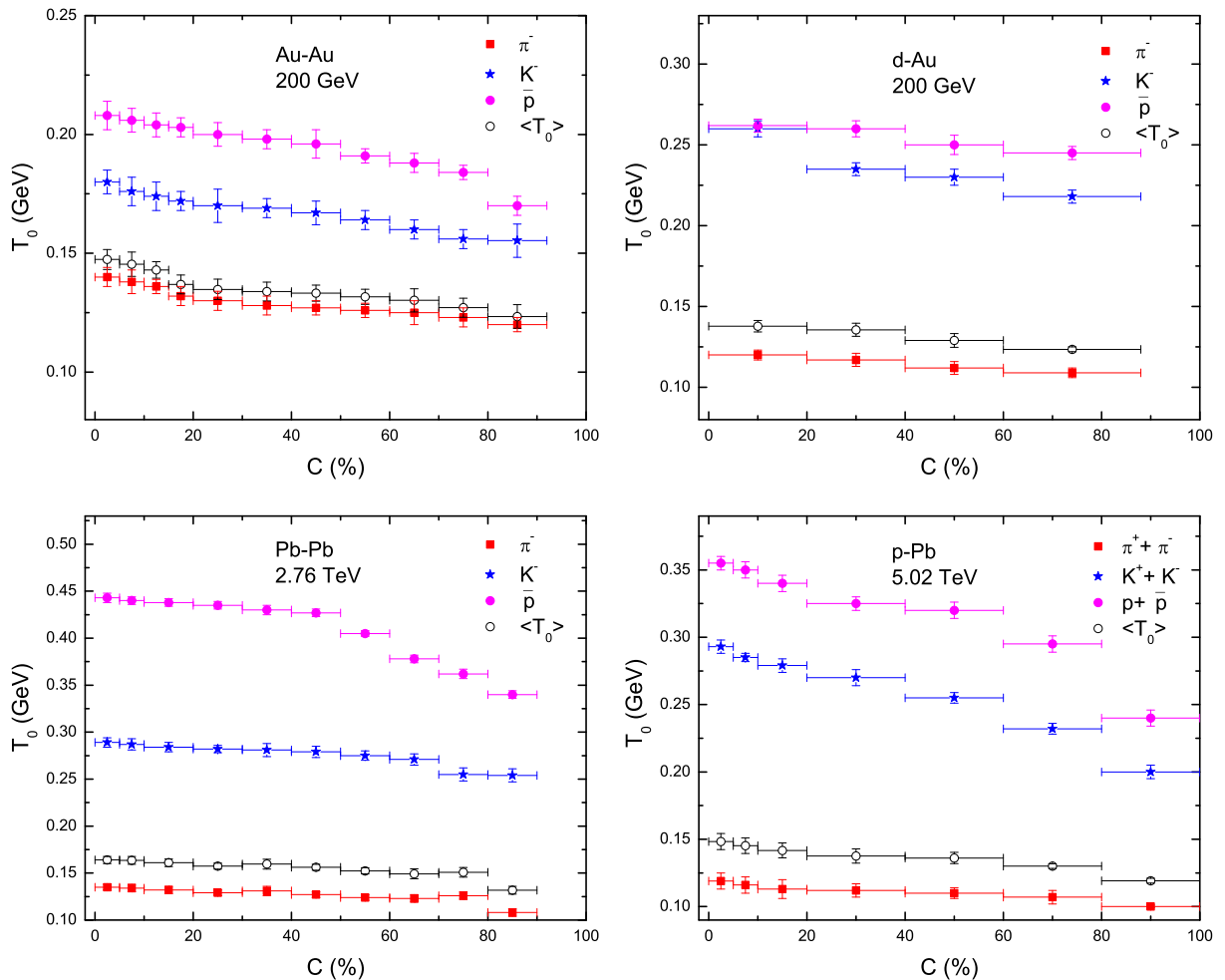


Fig. 3. Dependence of T_0 on event centrality percentage in 200 GeV Au-Au (left-upper), 200 GeV d -Au (right-upper), 2.76 TeV Pb-Pb (left-lower), and 5.02 TeV p -Pb (right-lower) collisions. Different symbols represent different parameter values listed in Tables 1 and 2. The weighted averages, $\langle T_0 \rangle$, over different particles are shown in the figure together.

range beyond which the thermal model does not work. In fact, the single thermal model works generally in low p_T region. For the spectra in high p_T region, we need another thermal component with high temperature, or the Hagedorn function [14, 15, 23, 24, 25] or its revisions [27, 28, 29, 30, 31].

Although the thermal model does not work in the region beyond the special p_T range, the Hagedorn function [14, 15], that is the inverse power-law [23, 24, 25] which is based on the quantum chromodynamics (QCD) theory, can be used to describe the spectra beyond the special p_T range. Because of the focus of the present work being the study of event centrality dependence of T_0 and β_T , we give up to describe the spectra beyond the special p_T range by using the Hagedorn function [14, 15]. Based on different pictures in physics, we can use different methods to describe the same p_T spectra. Different methods are expected to show similar or reconcilable results if only the spectra in the special p_T range are

considered [1, 2, 3, 4, 5, 6, 7, 8, 9, 10, 11, 12, 13].

In fact, we have another method to describe the spectra beyond the special p_T range. That is, a two-component thermal model in which the first component describes the spectra in the special p_T range and the second one describes the spectra beyond the special p_T range. As the fraction beyond the special p_T range is small, the two-component thermal model causes a small increase in T_0 and/or β_T . Because of the increase in T_0 and/or β_T being small in the two-component thermal model, we neglect the contribution of the second component in the extraction of T_0 and β_T , though the application of the two-component thermal model is expected to be more successful than that of the single thermal model.

The observed β_T increases slightly or does not change obviously with the increase of event centrality and collision energy. This is in agreement with most of the literature [1, 2, 3, 4], though the concrete values are different

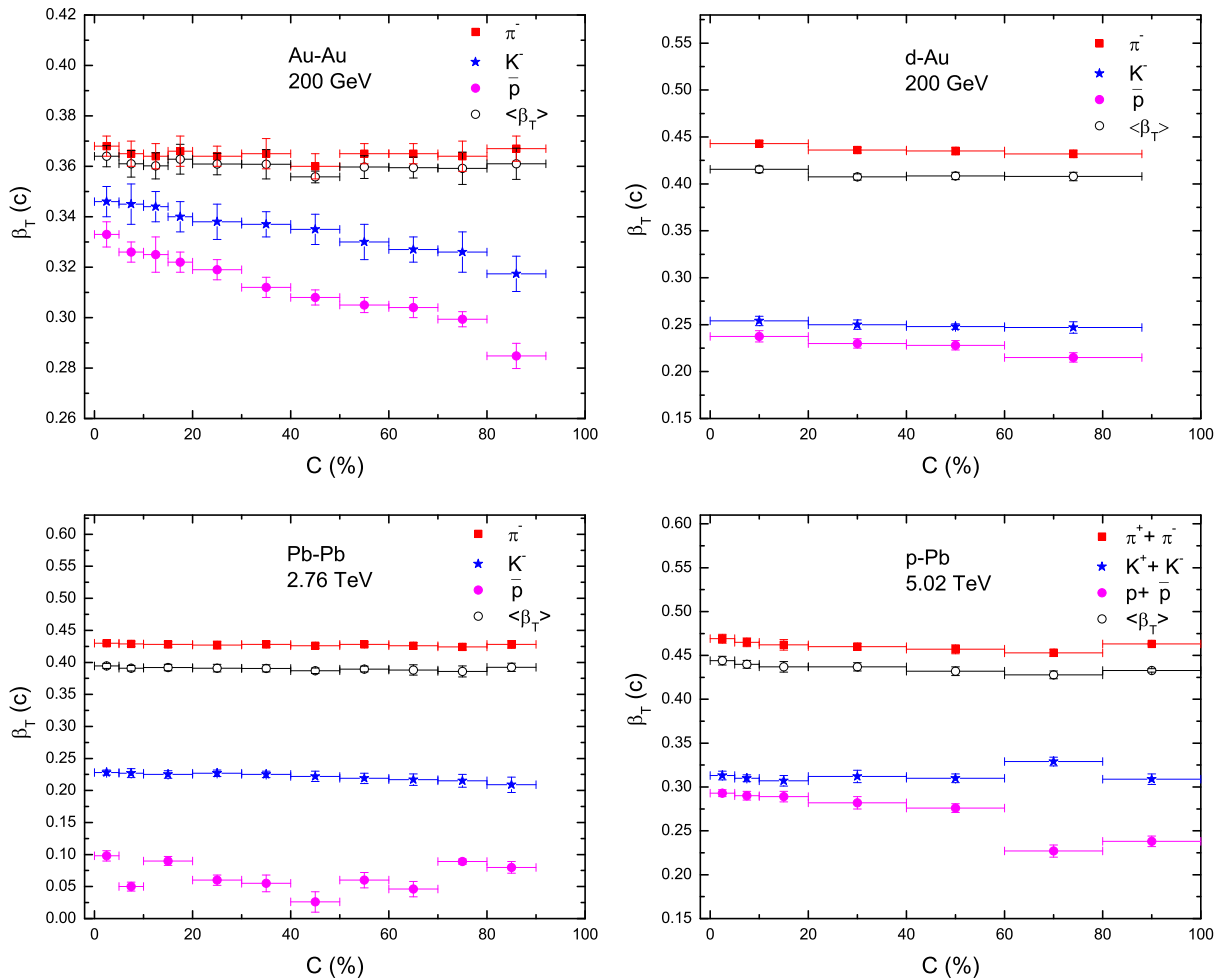


Fig. 4. Dependence of β_T on event centrality percentage in 200 GeV Au-Au (left-upper), 200 GeV *d*-Au (right-upper), 2.76 TeV Pb-Pb (left-lower), and 5.02 TeV *p*-Pb (right-lower) collisions. Different symbols represent different parameter values listed in Tables 1 and 2. The weighted averages, $\langle\beta_T\rangle$, over different particles are shown in the figure together.

from each other. The observed T_0 increases slightly or does not change obviously with the increase of event centrality and collision energy. This is inconsistent with some literature [1, 2, 3, 18, 40] and in agreement with others [4, 16, 44, 45, 46]. In particular, ref. [47] shows that T_0 extracted from pion spectra in central collisions is smaller than that in peripheral collisions, and that extracted from kaon or proton spectra does not depend on the centrality. Meanwhile, β_T in central collisions is larger. Our observation on β_T is in agreement with ref. [47]. In fact, due to the anti-correlation between T_0 and β_T for a given spectrum, the acceptable sets of free parameter values are not unique. This renders that the collision process is complex and more analysis is needed. Indeed, the present work uses particle-independent p_T range, fixed flow profile ($n_0 = 2$ as in ref. [1]), and small β_T change, which results in different T_0 trend with some literature [2, 18], though the same blast-wave model is used.

3.3 Further discussion

The above comparison renders that the event centrality and collision energy dependent T_0 (β_T) is complex if one fits the p_T spectra by the same or similar model, let alone different models. In particular, there exists lots of other models that go far beyond a blast wave approximation to describe the p_T spectra [48, 49], which are not always suitable to extract T_0 and β_T . In addition, some models do not extract directly T_0 and β_T [2, 5, 6, 7, 8, 9, 10, 11, 12, 13], though they describe the p_T spectra to extract the so-called effective temperature, T . Alternatively, T_0 is regarded as the intercept in the linear relation of T against m_0 , and β_T is regarded as the slope in the linear relation of $\langle p_T \rangle$ against mean energy (i.e. the mean moving mass \overline{m}).

In our opinion, if higher T_0 in central collisions and at the LHC signifies higher excitation degree of inter-

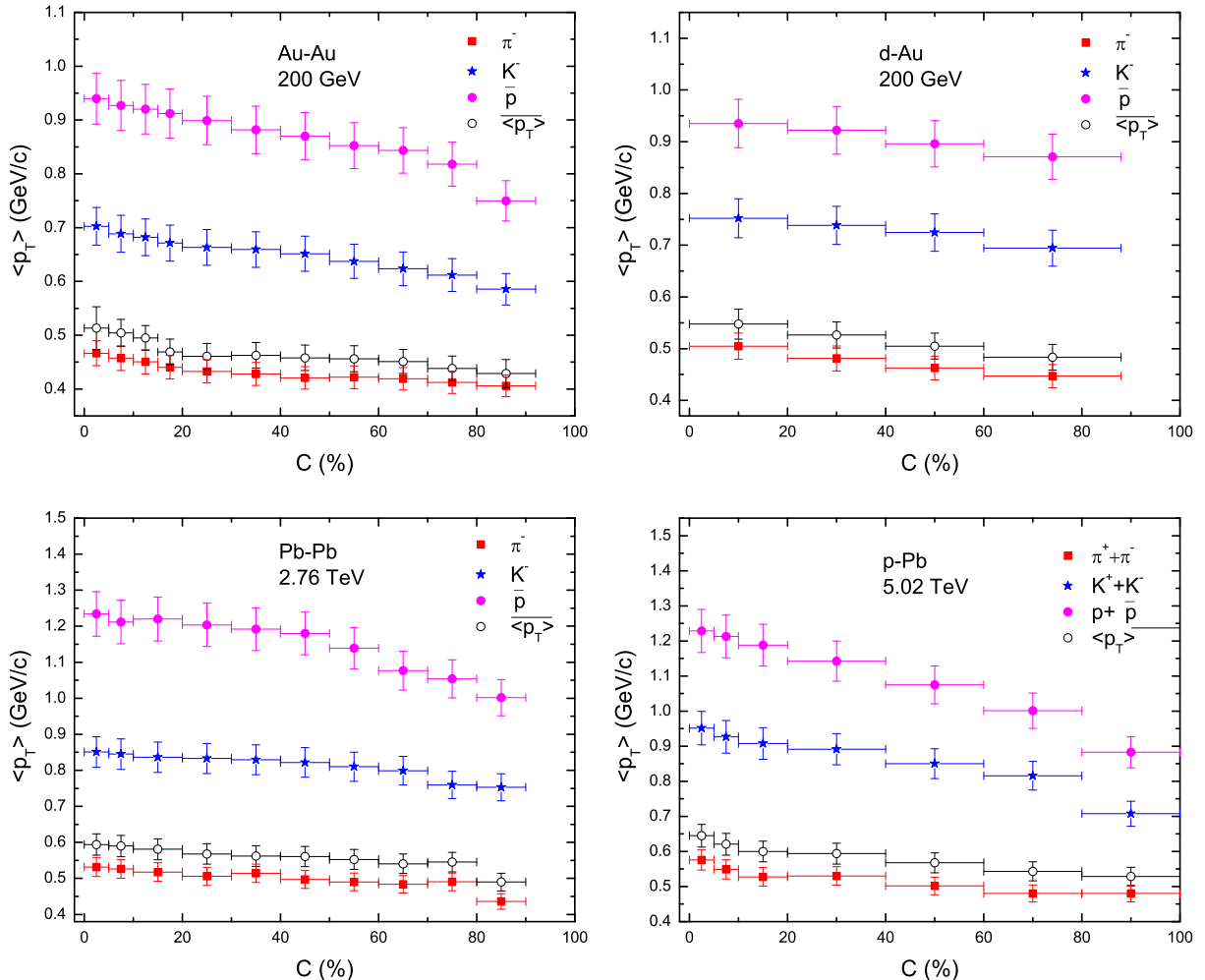


Fig. 5. Dependence of $\langle p_T \rangle$ on event centrality percentage in 200 GeV Au-Au (left-upper), 200 GeV *d*-Au (right-upper), 2.76 TeV Pb-Pb (left-lower), and 5.02 TeV *p*-Pb (right-lower) collisions. Different symbols represent the results for different particles based on the parameter values listed in Tables 1 and 2. The weighted averages, $\langle p_T \rangle$, over different particles are shown in the figure together.

acting system, lower T_0 in central collisions and at the LHC signifies longer lifetime of hot and dense matter in the case of considering higher excitation degree. Based on different pictures and functions, the values and tendency of T_0 (β_T) extracted from the same p_T spectra are possibly different from each other. The pictures and functions used the Boltzmann-Gibbs (Fermi-Dirac or Bose-Einstein) statistics and standard distribution have more potentials to be the unified ‘‘thermometer’’ and/or ‘‘speedometer’’ because they are the most similar to the ideal gas model in thermodynamics.

It should be noted that the above discussions are in the low p_T region. If we increase the region by a few GeV/ c , the conclusions do not change obviously due to the fact that the values of T_0 and β_T do not change obviously. In fact, the fraction of particles with high p_T is very small. Including particles with high p_T causes a little ($< 5\%$) increase in T_0 and/or β_T , where the $< 5\%$

statement is estimated by us due to little yield of particles from high p_T region. While decreasing p_T region by a few GeV/ c causes obvious change in T_0 and β_T due to the large change in fraction. As the parameters in the blast-wave model, T_0 and β_T are sensitive to p_T region contributed by the soft process and insensitive to p_T region contributed by the hard process.

To extract T_0 and β_T as accurately as possible, one may use some restrictions in the fit process. For example, the p_T region does not need to be very wide due to the fact that the fraction of particles with high p_T is very small. The rapidity should be in the central region. If the rapidity is in the fragmentation region, we may transform it to the central region so that the kinetic energy of directional movement can be eliminated from the total energy. The particles should be light flavor particles due to the heavy flavor particles being produced mainly in the non-thermal process. Anyhow, the same

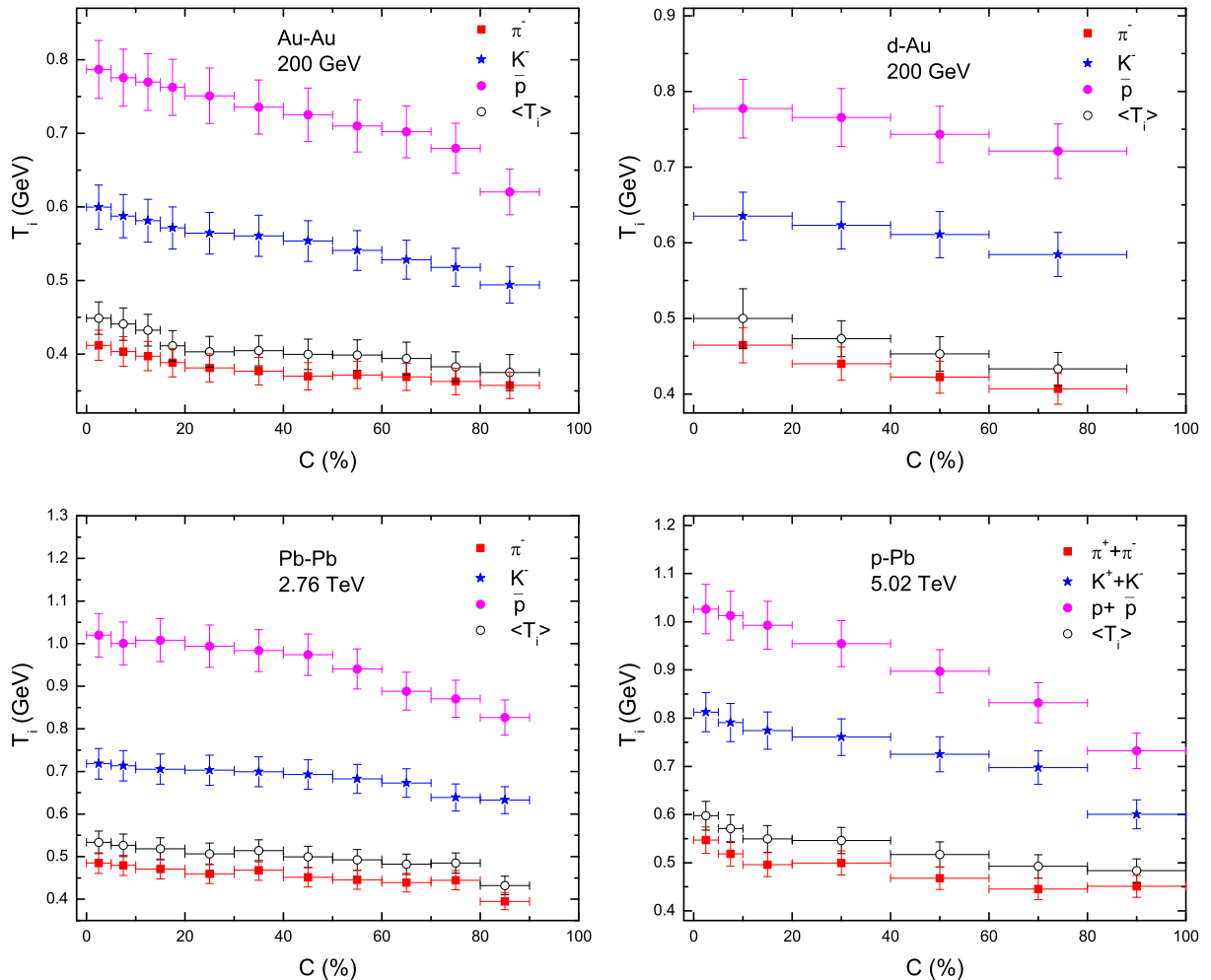


Fig. 6. Dependence of T_i on event centrality percentage in 200 GeV Au-Au (left-upper), 200 GeV d -Au (right-upper), 2.76 TeV Pb-Pb (left-lower), and 5.02 TeV p -Pb (right-lower) collisions. Different symbols represent the results for different particles based on the parameter values listed in Tables 1 and 2. The weighted averages, $\langle T_i \rangle$, over different particles are shown in the figure together.

p_T region should be used in different centralities for a given particle and system to obtain accurate results as far as possible.

No matter how large the correlation of T_0 and β_T is, $\langle p_T \rangle$ and T_i are independent of models and parameters if the models fit well the data. In fact, $\langle p_T \rangle$ and T_i are reflections of data sample itself in case if the models fit the data well. The results will be similar to Figs. 5 and 6 if we use other models to fit the data well. Considering two nucleons or partons taking part in each binary collision, the contribution fraction of each nucleon or parton to $\langle p_T \rangle$ is $1/2$. In the Erlang distribution, $\langle p_T \rangle/2$ is regarded as the temperature parameter [50]. If the contribution fraction of thermal motion to $\langle p_T \rangle/2$ is k_0 , we can obtain T_0 to be $k_0 \langle p_T \rangle/2$ and β_T to be $(1 - k_0) \langle p_T \rangle/2m_0\bar{\gamma}$, where $\bar{\gamma}$ denotes the mean Lorentz factor of the given particles in the source rest frame. Thus, we can obtain the similar trends of T_0 (β_T) to the blast-wave model.

The value of $\langle T_0 \rangle$ ($\langle \beta_T \rangle$, $\overline{\langle p_T \rangle}$, or $\langle T_i \rangle$) for different particles in Au-Au and d -Au collisions, as well as in Pb-Pb and p -Pb collisions, are similar to each other. These results confirm the maximum size dependent effect [33], which states that the main parameters such as the kinetic freeze-out temperature and transverse flow velocity are mainly determined by the heaviest nucleus from proton-nucleus to nucleus-nucleus collisions. In the maximum size dependent effect, the number of participant nucleons in collisions of single projectile proton with target nucleus plays a main role. This renders that central (peripheral) proton-nucleus and nucleus-nucleus collisions result in similar results to each other, and peripheral proton-nucleus and nucleus-nucleus collisions also result in similar results to proton-proton collisions.

Comparing with our previous work [33] which studies more models, the progress in this paper is obvious. In fact, the dependences of T_0 , β_T , $\langle p_T \rangle$, and T_i on centrality are studied in this paper in whole cen-

trality range. We confirm here that these dependences decrease monotonously from central to peripheral collisions, which is not always the case for T_0 in some cases if we use particle dependent p_T region and centrality dependent n_0 as used in current literature [1, 2, 3, 4, 45]. The “standard pictures” extracted from low to the highest energies in nuclear collisions show that T_0 increase from central to peripheral collisions. The difference in T_0 between our result and the “standard picture” is caused by the choice of p_T range and n_0 . In our opinion, T_0 and β_T depend on particle dependent p_T range and centrality dependent n_0 . We have used the fixed p_T range and invariable n_0 in this paper which results in different trend for T_0 from the “standard picture”. It is hard to say that which picture is more suitable.

Generally, at given collision energy and in given event centrality, larger system produces more particles. For a given collision system, with the increase of centrality, larger amount of particles are produced, and both T_0 and β_0 also become larger. It is expected that, not only for large system (e.g. Pb-Pb) but also for small system (e.g. p -Pb), the centrality classes that have similar average $dN/d\eta$ (or N_0) should have similar T_0 and β_0 . This paper confirms that medium and peripheral Pb-Pb collisions that produce similar amount of particles as central and medium p -Pb collisions also have similar T_0 and β_T . That is to say that, in central and medium p -Pb collisions, both T_0 and β_T are larger as those in medium and peripheral Pb-Pb collisions.

Before summary and conclusions, we would like to point out that the present work is a more systematic study on the dependence of T_0 (β_T , $\langle p_T \rangle$, or T_i) on centrality in Au-Au, d -Au, Pb-Pb, and p -Pb collisions at the RHIC and LHC by using the blast-wave model with Boltzmann-Gibbs statistics, though our previous work [51] studied T_0 (β_T , q (entropy index), p_0 , and n) in central and peripheral Au-Au and Pb-Pb collisions by using an improved Tsallis distribution [38, 52]. With regard to the relative size of T_0 (β_T) in central and peripheral collisions, the results from the two works are consistent with each other. However, the improved Tsallis distribution results in larger β_T which is inconsistent with the blast-wave model with Boltzmann-Gibbs statistics or with Tsallis statistics [53]. Thus, we did not use the improved Tsallis distribution in the present work. In addition, two components were used in our previous work [51] which resulted in good fit within and beyond the special p_T range, which is not the case in the present work which uses one component in fact.

In the above discussion on extracting T_0 and β_T , the influence of resonances if available are naturally included in the soft component. As discussed in ref. [1], the resonances change the slopes of the p_T spectra, which affect the values of T_0 and β_T . In some cases, the spectra in very low p_T region are not available in experi-

ments, which results in larger T_0 and β_T in the present work. Although the influence of resonances on particle yields are not too large [54], this influence on pions is the largest among the considered particles [54, 55]. To include the influence will result in lower T_0 and β_T for pions than for kaons and protons. This will strengthen further our conclusion on multiple kinetic freeze-out scenario in detailed analysis. Although the chemical freeze-out is single scenario in the traditional statistical thermal model [55, 56, 57, 58], the kinetic freeze-out is possibly mass dependent [10, 22, 37, 38]. In particular, in a very recent work [59], the two-scenario of chemical freeze-out is studied and the inclusion of additional resonances are not sufficient to close the gap between the chemical freeze-out temperatures for emissions of light and strange hadrons.

At the end of this discussion, we would like to point out that the value of T_0 obtained from the analysis (for heavier hadrons) is more than the value of critical temperature ($T_c \approx 170$ – 200 MeV) obtained in lattice QCD calculations [60, 61, 62]. This result does not mean that the kinetic freeze-out takes place before the phase transition. In fact, the value of $\langle T_0 \rangle$ is less than the value of T_c , if we consider averagely and generally. In addition, it is indeed that T_0 is a “true” kinetic freeze-out temperature but not the inverse slope of the spectra because the transverse flow velocity β_T is extracted out. However, T_0 and T_c are obtained from different “thermometers”. Meanwhile, the larger T_i for heavier hadrons emission comparing with that from other methods [63, 64, 65, 66] is also caused by different “thermometers”, though $\langle T_i \rangle$ is nearly the same as or close to refs. [64, 65, 66]. Before giving a quantitative comparison for different temperatures, one has to define a unified “thermometer”. This topic is beyond the focus of this paper. We shall not discuss it further.

4 Summary and conclusions

We summarize here our main observations and conclusions.

The centrality-dependent double-differential transverse momentum spectra of charged pions and kaons and (anti)protons produced in mid-(pseudo)rapidity interval in $\sqrt{s_{NN}} = 200$ GeV Au-Au and d -Au, 2.76 TeV Pb-Pb, and 5.02 TeV p -Pb collisions are analyzed by the blast-wave model with Boltzmann-Gibbs statistics. The model results are approximately in agreement with the experimental data in special transverse momentum ranges measured by the PHENIX and ALICE Collaborations.

There are special transverse momentum ranges in some transverse momentum spectra. The special transverse momentum range increases from $0 \sim 2$ – 3 GeV/ c

to $0 \sim 4.5$ GeV/ c or a little more when the event centrality increases from periphery to center. This range for the strange particle is narrower than that for the non-strange particle. The dependence of this range on collision energy is not obvious. The special transverse momentum ranges appear due to different fractions of participant nucleons in events with different centralities.

The kinetic freeze-out temperature and the transverse flow velocity increase slightly in some cases or do not change obviously in other cases with the increase of event centrality and collision energy. These outcomes result in faster or the same thermal motion and collective expansion in central collisions, at the LHC, and for large system. Comparing with central collisions, a large fraction in high transverse momentum region is observed in peripheral collisions due to large cascade scattering happen in spectator nucleons. The single thermal model does not describe simultaneously the spectra in both the low and high transverse momentum regions, though the two-component thermal model is expected to describe simultaneously the spectra in the two regions.

The average transverse momentum and initial temperature increase with the increase of event centrality, collision energy, and particle mass. With the increase of projectile size in the case of using the same target nucleus, the two quantities and main parameters (kinetic freeze-out temperature and transverse flow velocity) do not change obviously. This confirms the maximum size dependent effect, which states that the main parameters such as the kinetic freeze-out temperature and transverse flow velocity are mainly determined by the heaviest nucleus from proton-nucleus to nucleus-nucleus collisions.

The present work also confirms the multiple kinetic freeze-out scenario if we use the detailed analysis. Although the chemical freeze-out is single scenario in the traditional statistical thermal model, there is also two-scenario of chemical freeze-out studied in literature. The present work shows that the kinetic freeze-out is possibly particle mass dependent, which show an increase of kinetic freeze-out temperature with the increase of particle mass. If the influence of resonances can be measured in experiments in detail, the multiple kinetic freeze-out scenario is expected to strengthen further.

Acknowledgments

This work was supported by the National Natural Science Foundation of China under Grant Nos. 11575103 and 11947418, the Chinese Government Scholarship (China Scholarship Council), the Scientific and Technological Innovation Programs of Higher Education Institutions in Shanxi (STIP) under Grant No. 201802017, the Shanxi Provincial Natural Science Foundation under Grant No. 201901D111043, and the Fund for Shanxi “1331 Project” Key Subjects Construction.

Data availability

The data used to support the findings of this study are included within the article and are cited at relevant places within the text as references.

Compliance with ethical standards

Conflict of interest

The authors declare that there are no conflicts of interest regarding the publication of this paper. The funding agencies have no role in the design of the study; in the collection, analysis, or interpretation of the data; in the writing of the manuscript, or in the decision to publish the results.

References

- [1] E Schnedermann, J Sollfrank and U Heinz *Phys. Rev. C* **48** 2462 (1993)
- [2] B I Abelev et al. [STAR Collaboration] *Phys. Rev. C* **79** 034909 (2009)
- [3] B I Abelev et al. [STAR Collaboration] *Phys. Rev. C* **81** 024911 (2010)
- [4] Z B Tang, Y C Xu, L J Ruan, G van Buren, F Q Wang and Z B Xu *Phys. Rev. C* **79** 051901(R) (2009)
- [5] S Takeuchi, K Murase, T Hirano, P Huovinen and Y Nara *Phys. Rev. C* **92** 044907 (2015)
- [6] H Heiselberg, A M Levy *Phys. Rev. C* **59** 2716 (1999)
- [7] U W Heinz, arXiv:hep-ph/0407360 (2004)
- [8] R Russo *PhD Thesis* (Universita degli Studi di Torino, Italy) (2015), arXiv:1511.04380 [nucl-ex] (2015)
- [9] H-R Wei, F-H Liu and R A Lacey *Eur. Phys. J. A* **52** 102 (2016)
- [10] H-L Lao, H-R Wei, F-H Liu and R A Lacey *Eur. Phys. J. A* **52** 203 (2016)
- [11] H-R Wei, F-H Liu and R A Lacey *J. Phys. G* **43** 125102 (2016)
- [12] J Cleymans and D Worku *Eur. Phys. J. A* **48** 160 (2012)
- [13] H Zheng and L L Zhu *Adv. High Energy Phys.* **2016** 9632126 (2016)
- [14] R Hagedorn *Riv. Nuovo Cimento* **6**(10), 1 (1983)
- [15] B Abelev et al. [ALICE Collaboration] *Eur. Phys. J. C* **75** 1 (2015)
- [16] S S Adler et al. [PHENIX Collaboration] *Phys. Rev. C* **69** 034909 (2004)
- [17] A Adare et al. [PHENIX Collaboration] *Phys. Rev. C* **88** 024906 (2013)
- [18] B Abelev et al. [ALICE Collaboration] *Phys. Rev. C* **88** 044910 (2013)
- [19] B Abelev et al. [ALICE Collaboration] *Phys. Lett. B* **728** 25 (2014)
- [20] S Chatrchyan et al. [CMS Collaboration] *Eur. Phys. J. C* **72** 1945 (2012)
- [21] M K Suleymanov *Int. J. Mod. Phys. E* **27** 1850008 (2018)

- [22] M Waqas, F-H Liu, S Fakhraddin, M A Rahim *Indian J. Phys.* **93** 1329 (2019)
- [23] R Odorico *Phys. Lett. B* **118** 151 (1982)
- [24] G Arnison et al. [UA1 Collaboration] *Phys. Lett. B* **118** 167 (1982)
- [25] T Mizoguchi, M Biyajima and N Suzuki *Int. J. Mod. Phys. A* **32** 1750057 (2017)
- [26] K Aamodt et al. [ALICE Collaboration] *Phys. Lett. B* **693** 53 (2010)
- [27] A De Falco [for the ALICE Collaboration]. *J. Phys. G* **38** 124083 (2011)
- [28] I Abt et al. [HERA-B Collaboration] *Eur. Phys. J. C* **50** 315 (2007)
- [29] B Abelev et al. [ALICE Collaboration] *Phys. Lett. B* **710** 557 (2012)
- [30] B Abelev et al. [ALICE Collaboration] *Phys. Lett. B* **718** 295 (2012) and Corrigendum *Phys. Lett. B* **748** 472 (2015)
- [31] I Lakomov [for the ALICE Collaboration] *Nucl. Phys. A* **931** 1179 (2014)
- [32] B Abelev et al. [ALICE Collaboration] *Phys. Lett. B* **708** 265 (2012)
- [33] H-L Lao, F-H Liu, B-C Li, M-Y Duan and R A Lacey *Nucl. Sci. Tech.* **29** 164 (2018)
- [34] P Bozek, *AIP Conf. Proc.* **1422** 34 (2012)
- [35] M Alqahtani, D Almaalol, M Nopoush, R Ryblewski, M Strickland, *Nucl. Phys. A* **982** 423 (2019)
- [36] Y-L Yan, Y Cheng, D-M Zhou, B-G Dong, X Cai, B-H Sa, L P Csernai, *J. Phys. G* **40** 025102 (2013)
- [37] S Chatterjee and B Mohanty *Phys. Rev. C* **90** 034908 (2014)
- [38] D Thakur, S Tripathy, P Garg, R Sahoo and J Cleymans *Adv. High Energy Phys.* **2016** 4149352 (2016)
- [39] R Sahoo *Association of Asia Pacific Physical Societies Bulletin* **29**(4), 16 (2019)
- [40] I Melo and B Tomášik *J. Phys. G* **43** 015102 (2016)
- [41] L J Gutay, A S Hirsch, R P Scharenberg, B K Srivastava and C Pajares *Int. J. Mod. Phys. E* **24** 1550101 (2015)
- [42] A S Hirsch, C Pajares, R P Scharenberg and B K Srivastava *Phys. Rev. D* **100** 114040 (2019)
- [43] P Sahoo, S De, S K Tiwari and R Sahoo *Eur. Phys. J. A* **54** 136 (2018)
- [44] S Chatterjee, B Mohanty and R Singh *Phys. Rev. C* **92** 024917 (2015)
- [45] Z B Tang, L Yi, L J Ruan, M Shao, C Li, H F Chen, B Mohanty and Z B Xu *Chin. Phys. Lett.* **30** 031201 (2013)
- [46] D Thakur, S Tripathy, P Garg, R Sahoo and J Cleymans, Proceedings of the 11th Workshop on Particle Correlations and Femtoscopy (WPCF2015), 3–7 Nov. 2015, Warsaw, Poland, arXiv:1603.04971 [hep-ph] (2016)
- [47] B De *Eur. Phys. J. A* **50** 138 (2014)
- [48] N Armesto, N Borghini, S Jeon et al. (editors), S Abreu, S V Akkelin, J Alam et al. (authors) *J. Phys. G* **35** 054001 (2008)
- [49] S A Bass, M Bleicher, W Cassing, A Dumitru, H J Drescher, K Eskola, M Gyulassy, D Kharzeev, Y Kovchegov, Z Lin, D Molnar, J Y Ollitrault, S Pratt, J Rafelski, R Rapp, D Rischke, J Schaffner-Bielich, B Schlei, A Snigerev, H Sorge, D Srivastava, J Stachel, D Teaney, R Thews, S Vance, I Vitev, R Vogt, X N Wang, B Zhang and J Zimányi *Nucl. Phys. A* **661** 205 (1999)
- [50] W-J Xie *Chin. Phys. C* **35** 1111 (2011)
- [51] H-L Lao, F-H Liu and R A Lacey *Eur. Phys. J. A* **53** 44 (2017)
- [52] T Bhattacharyya, J Cleymans, A Khuntia, P Pareek and R Sahoo *Eur. Phys. J. A* **52** 30 (2016)
- [53] H-L Lao, F-H Liu, B-C Li and M Y Duan *Nucl. Sci. Tech.* **29** 82 (2018)
- [54] N Yu and X F Luo *Eur. Phys. J. A* **55** 26 (2019)
- [55] J Cleymans, B Kämpfer and S Wheaton *Phys. Rev. C* **65** 027901 (2002)
- [56] F Becattini, J Manninen and M Gaździcki *Phys. Rev. C* **73** 044905 (2006)
- [57] A Andronic, P Braun-Munzinger, K Redlich and J Stachel *Nucl. Phys. A* **789** 334 (2007)
- [58] J Cleymans, H Oeschler, K Redlich and S Wheaton *Phys. Rev. C* **73** 034905 (2006)
- [59] P Alba, V M Sarti, J Noronha-Hostler, P Parotto, I Portillo-Vazquez, C Ratti and J M Stafford, *Phys. Rev. C* **101** 054905 (2020)
- [60] M Cheng, N H Christ, S Datta, J van der Heide, C Jung, F Karsch, O Kaczmarek, E Laermann, R D Mawhinney, C Miao, P Petreczky, K Petrov, C Schmidt, W Soeldner and T Umeda, *Phys. Rev. D* **77** 014511 (2008)
- [61] A Bazavov, T Bhattacharya, M Cheng, N H Christ, C DeTar, S Ejiri, S Gottlieb, R Gupta, U M Heller, K Huebner, C Jung, F Karsch, E Laermann, L Levkova, C Miao, R D Mawhinney, P Petreczky, C Schmidt, R A Soltz, W Soeldner, R Sugar, D Toussaint and P Vranas, *Phys. Rev. D* **80** 014504 (2009)
- [62] Y Aoki, Z Fodor, S D Katz and K K Szabo, *J. High Energy Phys.* **0601** 089 (2006)
- [63] R A Soltz, I Garishvili, M Cheng, B Abelev, A Glenn, J Newby, L A L Levy and S Pratt, *Phys. Rev. C* **87** 044901 (2013)
- [64] M Csanád, Proceedings of the 7th Workshop on Particle Correlations and Femtoscopy (WPCF2011), 20–24 Sept. 2011, Tokyo, Japan, *PoS WPCF2011* 035 (2011), arXiv:1202.5974 [nucl-th] (2012)
- [65] J K Nayak, J Alam, S Sarkar and B Sinha, *J. Phys. G* **35** 104161 (2008)
- [66] D K Srivastava, R Chatterjee and M G Mustafa, arXiv:1609.06496 [nucl-th] (2016)